Regional chronostratigraphic synthesis of the Cenomanian-Turonian OAE2 interval, Western Interior Basin (USA): New Re-Os chemostratigraphy and $^{40}Ar/^{39}Ar$ geochronology

Matthew M. Jones[a*1], Bradley B. Sageman[a], David Selby[b,c], Brian R. Jicha[d], Brad S. Singer[d], Alan L. Titus[e]

[a]Department of Earth and Planetary Sciences, Northwestern University, Evanston, IL, USA 60208 mmjgeo@umich.edu, b-sageman@northwestern.edu

[b]Department of Earth Sciences, Durham University, Durham, DH1 3LE, UK

[c]State Key Laboratory of Geological Processes and Mineral Resources, China University of Geosciences, Wuhan 430074, China

[d]Department of Geoscience, University of Wisconsin-Madison, 1215 W. Dayton St., Madison, WI, USA 53706 brian.jicha@wisc.edu, bsinger@geology.wisc.edu

[e]Grand Staircase – Escalante National Monument, Bureau of Land Management, Kanab, UT, USA 84741 atitus@blm.gov

*Corresponding author; [1]Present address: Department of Earth and Environmental Sciences, University of Michigan, Ann Arbor, MI, USA 48109 mmjgeo@umich.edu

Highlights:

- New bentonite $^{40}Ar/^{39}Ar$ dates yield revised Cenomanian-Turonian Boundary (CTB) age
- New rhenium-osmium geochemistry of Angus and SH#1 cores in Western Interior Basin
- Rapid pre-OAE2 initial Os isotope excursions mark large igneous province volcanism
- 59±10 kyr lag between LIP volcanism and global net organic C burial at OAE2 onset
- Quantified duration of basal OAE2 hiatus in the Base Turonian GSSP section at Pueblo, CO

Keywords:

- Ocean Anoxic Event 2, geochronology, Cenomanian-Turonian stage boundary, large igneous province volcanism, osmium chemostratigraphy, Western Interior Seaway

Abstract

Fluctuations in depositional conditions during the onset of severe climate events in Earth history predispose stratigraphic archives to hiatuses, often hindering complete reconstructions of paleoclimate events and their triggers. Several studies have proposed that a hiatus of unknown duration exists at the base of Oceanic Anoxic Event 2 (OAE2) in the North American Western Interior Basin (WIB) at the Base Turonian Global Boundary Stratotype Section and Point (GSSP) in Pueblo, Colorado, potentially influencing integrated radioisotopic, biostratigraphic, and astrochronologic age models of the Cenomanian-Turonian boundary (CTB) interval. To quantify the duration of this hiatus, refine the chronology of OAE2, and assess marine geochemical perturbations associated with the onset of the event, we present new $^{40}Ar/^{39}Ar$ dates from regional CTB interval bentonites along with a new proximal-distal chemostratigraphic transect of the epeiric WIB, including rhenium-osmium and stable carbon isotope data. The new $^{40}Ar/^{39}Ar$ age determinations confirm and further constrain previous estimates of CTB timing. Initial osmium isotope ratio (Os_i) studies of OAE2 at globally distributed sites record prolific large igneous province (LIP) volcanic activity 10's of kyr prior to the carbon isotope ($\delta^{13}C$) excursion of OAE2. However, a recent chemostratigraphic study observed minimal stratigraphic offset between Os_i and $\delta^{13}C$ excursions in a Re-Os record near the Base Turonian GSSP in the central WIB, confirming a hiatus. In contrast, the new Os_i chemostratigraphy of the Angus Core (Denver Basin) and SH#1 Core (S. Utah) exhibit more characteristic stratigraphic lags between Os_i and $\delta^{13}C$ excursions, indicating stratigraphic expansion and conformability across the onset of the event at other sites in the WIB. An existing astronomical time scale for the Angus Core quantifies the temporal lag between LIP volcanism and the beginning of OAE2 (59±10 kyr) and constrains the duration of the hiatus in the Portland Core as geologically brief, indicating that the stratigraphic

record at the GSSP locality is largely conformable through OAE2. This astronomically-tuned conformable Os_i record across the onset of OAE2 captures a geologically rapid onset of LIP volcanism, consistent with other records, such that the addition of CO_2 to the ocean-atmosphere system may have driven changes in marine carbonate chemistry. Additionally, the refined chronostratigraphy of OAE2 and the CTB in the central WIB improves correlation with other records, such as those in the Eagle Ford Group, Texas. The correlations highlight that discrepancies among OAE2 age models from globally distributed sections commonly stem from differing definitions of the event and uncertainties associated with astronomical tuning, in addition to stratigraphic preservation.

INTRODUCTION AND BACKGROUND

Resolving the causal mechanisms of major paleoclimate and paleobiotic events in Earth history is critical to understanding the vulnerabilities of modern and ancient ecosystems. However, the extreme changes in depositional environments associated with the onset of many mass extinction events and carbon cycle perturbations, such as sea level fluctuations or ocean acidification, may result in hiatal surfaces that obscure geological evidence of the processes initiating such events (Smith et al., 2001; Holland and Patzkowsky, 2015; Baresel et al., 2017). Expanded, or at least relatively continuous, stratigraphic successions with robust time control are, therefore, key to reconstructing climate change in the geologic record. This study investigates the onset of Oceanic Anoxic Event 2 (OAE2, ~94 Ma), a significant Late Cretaceous carbon cycle perturbation lasting over half a million years, through a proximal-distal chemostratigraphic transect of the shallow marine Western Interior Basin (WIB) of North America. It assesses stratigraphic conformability at reference sites such as the Base Turonian Stage Global Boundary Stratotype Section and Point (GSSP) in Pueblo, Colorado, and refines the timing of changes in volcanic activity, global geochemical cycles, and sea level spanning the onset of OAE2.

Episodes of voluminous volcanism emplacing large igneous provinces (LIPs) commonly precede, or are broadly contemporaneous with, carbon cycle perturbations and mass extinctions through geologic time (Wignall, 2001; Turgeon and Creaser, 2008; Kidder and Worsley, 2010). As a result, elemental and isotopic paleoceanographic proxies sensitive to volcanic fluxes may identify the initiation of such events, as well as elucidate a causal linkage between LIPs and perturbation of the carbon cycle. Moreover, they provide potential chemostratigraphic markers to define the relative expansion or condensation of stratigraphic intervals during the onset of such events, arguably the critical phase for determination of causal factors. This is especially the case for isotopic systems with short marine residence times (τ) that capture rapid changes in geochemical fluxes (e.g., Kuroda et al., 2007; Percival et al., 2018). The osmium reservoir of the global ocean mixes over geologically brief time scales (τ < 30 kyr, Oxburgh, 2001; Rooney et al., 2016) and, at the time of deposition, initial marine osmium isotope ratios ($^{188}Os/^{187}Os_{(initial)} = Os_i$) principally record changes in the relative fluxes of osmium from two isotopically distinct end members, continental weathering (Os_i = ~1.4) and hydrothermal inputs (Os_i = 0.13) (Peucker-Ehrenbrink and Ravizza, 2000). Consequently, the Os_i proxy has resolved anomalous increases in volcanic activity across many Mesozoic climate transitions, including OAEs, the Triassic-Jurassic Boundary, and the Cretaceous-Paleogene Boundary (Ravizza and Peucker-Ehrenbrink, 2003; Kuroda et al., 2010; Bottini et al., 2012).

For OAE2, the discovery of an abrupt unradiogenic Os_i excursion at the base of the event (Turgeon and Creaser, 2008) provides strong evidence for the hypothesis that hydrothermal inputs, likely emanating from the Caribbean LIP and potentially the High Arctic LIP, triggered an Earth system response that ultimately led to expanded bottom water anoxia and elevated organic carbon burial (Sinton and Duncan, 1997; Kerr, 1998; Snow et al., 2005; Adams et al., 2010; Barclay et al., 2010; Owens et al., 2013). The OAE2 Os_i excursion is also recorded in numerous disparate basins, confirming the proxy as a globally correlative marine chemostratigraphic marker and highlighting a temporal lag, on the order of tens of kiloyears, between the onset of the Os_i excursion and the younger carbon isotope ($\delta^{13}C$) excursion (Turgeon and Creaser, 2008; Du Vivier et al., 2014; Du Vivier et al., 2015b; Schröder-Adams et al., 2019; Sullivan et al., in press). This lag likely reflects the fundamental response time of the Earth's carbon cycle to a massive pulse of CO_2 to the ocean-atmosphere system from LIP volcanism.

To assess the potential explanations and implications of this lag, and to quantify its duration, this study presents new Os_i chemostratigraphic records of the OAE2 onset interval in the WIB from the Angus Core in north-central Colorado and the SH#1 Core in southern Utah (Fig. 1). New $^{40}Ar/^{39}Ar$ dating of regionally correlated bentonites, along with existing radioisotopic ages, astrochronology, and $\delta^{13}C$ chemostratigraphy (Meyers et al., 2012b; Ma et al., 2014; Jones et al., 2019), provide tight age control at these locales for comparison with the Base Turonian GSSP in Pueblo, Colorado, as well as refine the timing and sequence of marine geochemical events through the onset of OAE2. A previous Os_i chemostratigraphy of the Portland Core, near the GSSP locality, does not exhibit the full characteristic lag between Os_i and $\delta^{13}C_{org}$ preserved in many other records globally (Du Vivier et al., 2014). This chemostratigraphic feature suggests that a hiatus exists at the base of OAE2 in the GSSP. As a result, some recent studies have questioned the stratigraphic completeness of the CTB records from the mid-latitudes of the WIB and suggested that critical time intervals of OAE2 may be missing at the GSSP (Eldrett et al., 2017; Li et al., 2017; Scott et al., 2018). Thus, the new Os_i chemostratigraphic transect of the WIB presents an opportunity to constrain the spatial extent, origin, and duration of this stratigraphic gap and to evaluate the hypothesis that a crucial interval of time is missing from sedimentary records of OAE2 in the central WIB, including at the GSSP locality.

GEOLOGIC SETTING AND MATERIALS

Cenomanian-Turonian Stratigraphy in the Western Interior Basin

The Late Cretaceous Greenhorn Cyclothem of the foreland Western Interior Basin preserves a ~10-Myr succession of shallow marine facies; OAE2 spans the CTB and occurs just prior to the Early Turonian peak highstand (maximum transgression) of the cyclothem (Kauffman and Caldwell, 1993). This highstand of the seaway inundated the North American craton and linked the proto-Gulf of Mexico to the arctic Boreal Sea, ranging longitudinally from present-day Iowa to central Utah (Fig. 1). Uplift along the Sevier thrust belt generated maximum subsidence in the proximal western foredeep of the basin, providing accommodation space and sediment supply that produced relatively expanded records of OAE2, such as in the Tropic Shale of the SH#1 Core near Big Water, Utah (Jones et al., 2019). Further east, in the more distal "axial basin" of Colorado and the "stable craton" of the central plains (*sensu* Kauffman, 1984), the hemipelagic sediments of the Bridge Creek Limestone accumulated more slowly and are more carbonate-rich. This is the case in the Angus Core of the Denver Basin, studied here, and in the Portland Core, near the Base Turonian GSSP at the Rock Canyon Anticline in Pueblo, Colorado (Figs. 1-2). A chronostratigraphic framework to correlate these proximal-distal mid-latitude regions of the WIB comprises: areally expansive and radioisotopically dated bentonites ("bentonites A-D"; Elder, 1988; Obradovich, 1993; Meyers et al., 2012b), ammonite, inoceramid, and microfossil biostratigraphy (Leckie, 1985; Bralower, 1988; Elder, 1989; Elder, 1991; Kauffman et al., 1993; Kennedy et al., 2005; Corbett and Watkins, 2013), astrochronology from climatically sensitive lithologic patterns (Sageman et al., 1997; Meyers et al., 2001; Ma et al., 2014; Jones et al., 2019), lithostratigraphy (Hattin, 1971; Cobban and Scott, 1972; Elder et al., 1994; Elderbak and Leckie, 2016), and carbon isotope chemostratigraphy (Pratt and Threlkeld, 1984; Pratt et al., 1993; Sageman et al., 2006; Joo and Sageman, 2014).

Prior to OAE2, during deposition of the late Cenomanian Hartland Shale in the axial basin, the seaway was relatively oxygen-depleted, restricted, and conducive to organic carbon burial (Eicher and Worstell, 1970; Sageman, 1985; Sageman, 1989; Meyers et al., 2001; Sageman et al., 2014a; Eldrett et al., 2017). The lower Bridge Creek Limestone overlies the Hartland Shale in the

Angus and Portland cores (Fig. 2) of the axial basin and preserves the carbon isotope excursion (CIE) that defines OAE2 globally (Pratt et al., 1993). The shift to more calcareous, rhythmically bedded lithologies above the basal contact of the Bridge Creek follows a transgression and pronounced backstepping of the basin's shoreline along the seaway's western margin in southern Utah (Kauffman, 1977; Laurin and Sageman, 2007). This deepening is associated with development of a more oxic watermass in the seaway during early OAE2 deposition in the lower Bridge Creek (Eicher and Worstell, 1970; Eicher and Diner, 1985, 1989; Arthur and Sageman, 1994; Savrda and Bottjer, 1994; Sageman et al., 1997; Eldrett et al., 2017), contrasting with anoxic conditions in many proto-Atlantic and Tethyan sites during the event (Schlanger et al., 1987).

Along the western paleo-margin of the seaway in southern Utah, the fossiliferous Tropic Shale overlies the Naturita Sandstone (Young, 1965; Peterson, 1969; Uličný, 1999), a unit that was, until recently, designated the Dakota Sandstone following standard lithostratigraphic convention for the WIB (Carpenter, 2014). The SH#1 Core, drilled near Big Water, UT on the Kaiparowits Plateau, records an apparently continuous succession of proximal calcareous shales through OAE2 and the CTB (Jones et al., 2019). Thin traceable carbonate-rich beds also occur within the OAE2 interval of the lower Tropic Shale in SH#1 and nearby outcrops, such as the Nipple Creek outcrop section sampled in this study for $^{40}Ar/^{39}Ar$ bentonite dating. The carbonate beds preserve evidence of partial diagenetic alteration within the expanded $\delta^{13}C$ chemostratigraphy of the SH#1 Core. This diagenesis relates to eccentricity paced relative sea level cycles and flooding surfaces (Jones et al., 2019), which grade westward to shoreface parasequences (Laurin et al., 2019) and eastward to the rhythmically bedded marlstone-limestone couplets of the Bridge Creek in the axial basin (Elder et al., 1994). The combined astrochronology, microfossil datums, bentonite A-D stratigraphy, expanded $\delta^{13}C$ chemostratigraphy (Jones et al., 2019), and ammonite biostratigraphy from outcrops on the Kaiparowits Plateau region (Elder, 1989) form a chronostratigraphic framework for the SH#1 Core within which our new Os_i chemostratigraphy and $^{40}Ar/^{39}Ar$ geochronologic data are incorporated.

OAE2 Hiatuses in the Central Western Interior Basin

The Bridge Creek and uppermost Hartland Shale in the Portland Core and GSSP exhibit evidence for hiatal surfaces at two horizons (Fig. 5). The first hiatal surface, identified by spectral analyses and quantified to be <20 kyr, occurs near the base of the ammonite *Neocardioceras juddi* Biozone (Meyers and Sageman, 2004). The second hiatus, a focus of this study, is associated with a phosphatic bone bed at the base of the CIE and 55 cm below the thick lowermost Bridge Creek limestone bed (Bed 63 or LS1) (Pratt, 1984; Eicher and Diner, 1989), which defines the members' contact (Cobban and Scott, 1972; Elder and Kirkland, 1985). This unquantified hiatus (Du Vivier et al., 2014) falls at the critical OAE2 onset interval (Fig. DR4 in the GSA Data Repository[1]).

METHODS

Re-Os Geochemistry

Existing $\delta^{13}C$ chemostratigraphic profiles guided high-resolution sampling for rhenium-osmium geochemical analyses through the onset of OAE2 from the SH#1 Core (n=20, median spacing = 50 cm) and the Angus Core (n=15, median spacing = 30 cm). See Data Repository for details on sample collection and alignment of the Angus Core depth scale with previous studies. Prior to analysis at Durham University, samples were powdered in ceramic containers using high-purity crushing techniques (Ottawa sand pre-clean) at Northwestern University. Following the methodology of Selby and Creaser (2003), sample powders were spiked with a $^{185}Re+^{190}Os$ tracer solution and digested in sealed Carius tubes with 8 mL of 0.25 g/g CrO_3 in 4N H_2SO_4 for ~48 hours at 220°C, principally leaching hydrogenous Re and Os (i.e., carbonates and organic matter). The Re fraction was isolated via NaOH-acetone extraction and anion chromatography. The Os fraction was isolated and purified via chloroform extraction with back reduction into HBr and $CrO_3 \cdot H_2SO_4$-HBr microdistillation. Isotopic ratios of samples and standards were measured on a Triton TIMS in negative ionization mode. The average 2σ precision for Os_i values was ± 0.014 (max = ± 0.057). Present-day measured $^{187}Os/^{188}Os$ values of samples were corrected to initial osmium ratios (Os_i) by accounting for post-depositional beta decay of ^{187}Re ($\lambda = 1.666 \times 10^{-11} yr^{-1}$; Smoliar et al., 1996) using an age of 94.4 Ma for the onset of OAE2.

$^{40}Ar/^{39}Ar$ Geochronology

Bulk samples of regional bentonites B, C, and D of (Elder, 1988) were collected from the Nipple Creek (NC) outcrop section in southern Utah 13 km WSW of the SH#1 Core (Fig. DR3 in the Data Repository). Bentonites were identified via the local lithostratigraphy of the CTB interval (Elder, 1991) and an impression of ammonite *N. juddi* confirmed the Bentonite B horizon. Two additional $^{40}Ar/^{39}Ar$ dates were obtained from samples of bentonites C and D previously collected and analyzed from Pueblo, Colorado (K-07-01C) and Lohali Point, Arizona (90-O-34) (Obradovich, 1993; Meyers et al., 2012b). Sanidine was isolated via magnetic and density sorting techniques and its composition verified using a variable pressure scanning electron microscope. Sanidine separates were irradiated for 65 hours along with the 28.201 Ma Fish Canyon Tuff sanidine (Kuiper et al., 2008) in the CLICIT facility of the Oregon State University TRIGA reactor. In the WiscAr Laboratory at the University of Wisconsin-Madison, individual sanidine crystals from each of the Nipple Creek bentonites were incrementally heated using a 50W CO_2 laser and the extracted gas analyzed using a Nu Instruments Noblesse multi-collector mass spectrometer following Jicha et al. (2016). Single crystal total fusion experiments were performed for samples K-07-01C and 90-O-34. Dates were calculated using the decay constants of Min et al. (2000) and reported with uncertainties as ±X/Y at the 95% confidence level with: (X) analytical sources of uncertainty including the *J* uncertainty and (Y) full external sources of uncertainty, including standard age and decay constants.

RESULTS

Re-Os Geochemistry

The new records from the Angus and SH#1 cores reproduce an abrupt, unradiogenic Os_i excursion that spans the onset of OAE2, similar to the Portland Core Os_i record (Du Vivier et al., 2014). Unlike the Portland Core record, however, both the SH#1 and Angus cores preserve strata between the bases of the Os_i and $\delta^{13}C$ excursions, as is documented in other conformable records of the OAE2 onset, such as the expanded Pont'd Issole section of southern France (Du Vivier et al., 2014). The Os_i excursion occurs below the base of the carbon isotope excursion (CIE) by 131±22 cm in the SH#1 Core at 122.29 m and by 80±25 cm in the Angus Core at 2279.98 m (Figs. 3-4 and Fig. DR4). The unradiogenic Os_i shift occurs in the SH#1 Core at a flooding surface ("fs2a" of Elder et al., 1994) (Fig. 4) and in the Angus Core in the uppermost calcareous shales of the Hartland Member.

Minimum values of Os_i at each Western Interior locality (SH#1 = 0.149 ± 0.006, Angus = 0.167 ± 0.002, Portland = 0.156 ± 0.003) approach the hydrothermal end member of the osmium isotope system ($^{187}Os/^{188}Os_{hydrothermal}$ = 0.13; Peucker-Ehrenbrink and Ravizza, 2000). However, the magnitude of the Os_i excursion is significantly larger in the proximal SH#1 Core (ΔOs_i = 1.30) than in the Portland Core (ΔOs_i = 0.78; Du Vivier et al., 2014) and the Angus Core (ΔOs_i = 0.74), due to more radiogenic Os_i values preceding the event (max. Os_i in SH#1 = 1.446 ± 0.039 vs. Angus = 0.910 ± 0.027) (Fig. 5).

The astronomical time scale for the Angus Core (Ma et al., 2014) constrains the duration of the temporal lag between the Os_i excursion and the base of the OAE2 CIE to 2.9 ± 0.5 precessional cycles, equivalent to 59 ± 10 kiloyears (Fig. 5). The Os_i and $\delta^{13}C$ excursions are nearly superimposed in the Portland Core, whereas initiation of the $\delta^{13}C$ shift lags the Os shift at the two other WIB sites. This observation supports the hypothesis of a hiatus in the Pueblo area and permits the duration of missing time to be quantified. Equivalent to the duration of the lag, the hiatus represents ~60 kyr (see Discussion). Based on the established astrochronology of the Angus Core, values of Os_i remain unradiogenic for 172-257 kiloyears spanning the ammonite *Sciponoceras gracile* Biozone at the beginning of OAE2 (Fig. 6).

Broadly correlative enrichments of Os, best represented by ^{192}Os concentration data, occur through the onset of OAE2 in all WIB sites (Figs. 2-3). Concentrations of ^{192}Os in the Angus Core are significantly enriched (max [^{192}Os] = 1183.9 ± 4.3 ppt) by roughly an order of magnitude compared to the SH#1 Core (max [^{192}Os] = 162.3 ± 0.9 ppt) (Table 1). Elevated ^{192}Os concentrations occur throughout the duration of the unradiogenic Os_i excursion.

Concentrations of Re in the Angus Core are highest in the uppermost Hartland Shale (max [Re] = 89.31 ± 0.22 ppb) in the ~60 kiloyears prior to OAE2 and exceed the background levels of

~50 ppb (Table 1; Figs. 4, 6). Similar to records from the Portland Core (Du Vivier et al., 2014), Re concentrations in the Angus Core decrease markedly above the Hartland Shale-Bridge Creek Limestone contact and during the main body of the OAE2 CIE. Like ^{192}Os, concentrations of Re are elevated in the central axial basin localities compared to the SH#1 core where Re concentrations do not exceed 14 ppb despite enrichment during the Os_i excursion.

$^{40}Ar/^{39}Ar$ Geochronology

The $^{40}Ar/^{39}Ar$ analyses yield five new precise sanidine $^{40}Ar/^{39}Ar$ dates for bentonites B, C and D (Table 2; Fig. 7). Incremental heating experiments produce plateau dates in most cases, with only one being markedly older than the population of plateau dates for a given sample. The weighted mean ages for each bentonite obey superposition and the ages for the B and C bentonites from different localities are indistinguishable (Table 2). Full analytical results and Ar plots can be found in the Data Repository (Tables DR4-5).

DISCUSSION AND IMPLICATIONS

Assessing Conformability of the Base Turonian GSSP

An integrated chronostratigraphic framework of radioisotopic age dates, astrochronology, chemostratigraphy, and biostratigraphy spans the Cenomanian-Turonian boundary (CTB) interval at the Base Turonian GSSP at Rock Canyon Anticline in Pueblo, Colorado, constraining rates of change in geochemical and paleobiologic datasets from the Western Interior Seaway during OAE2 (Kennedy et al., 2005; Sageman et al., 2006 and refs therein). This high-resolution age control has aided in quantifying a cryptic 17 kyr hiatus above the LS5 bed of Elder et al. (1994) in the Bridge Creek Limestone Member (Meyers and Sageman, 2004) and has also indicated the presence of a second hiatus at the base of OAE2 at the GSSP section, assessed in this study (Fig. 5). This basal OAE2 hiatus occurs as a distinct 0.5 cm "thin wavy-bedded layer" in the uppermost Hartland Shale with phosphatized bones and scoured quartz sand at the GSSP (Pratt, 1984). These sedimentological characteristics, along with a sharp influx of benthic foraminifera with Tethyan affinity in the overlying uppermost marlstone bed of the Hartland Shale, allude to a marked shift in paleoenvironmental conditions which Eicher and Diner (1989) hypothesized to represent a hiatus. More recently, Os_i chemostratigraphy of the nearby Portland Core (Fig. 5) detected that the unradiogenic Os_i excursion preceding OAE2 directly underlies the base of the event's CIE and lacks the characteristic stratigraphic lag between Os_i and $\delta^{13}C$ excursions of the event globally(Du Vivier et al., 2014). This chemostratigraphic feature confirmed the presence of a hiatus (Fig. DR4 in Data Repository) that has the potential to impact geochemical reconstructions of the critical OAE2 onset interval and precise Earth system responses to the event's trigger (see discussion in Du Vivier et al., 2015a; Eldrett et al., 2017). However, the duration of the hiatus at the base of the OAE2 CIE at the GSSP section and Portland Core remained unquantified prior to this study.

Lithostratigraphic correlations of the hemipelagic marlstone-limestone couplets of the CTB interval in the central WIB reveal that the LS1 bed of the Bridge Creek at the GSSP and Portland Core is condensed (Ma et al., 2014). The bed expands into multiple couplets south and north of Pueblo, at the Greenhorn Creek outcrop and in the Angus Core of the Denver Basin, respectively (Fig. 5). Additionally, the new Os_i chemostratigraphy of the CTB interval from both the SH#1 Core and the astronomically-tuned Angus Core exhibit an expanded stratigraphic interval between the Os_i excursion and base of the OAE2 CIE (Figs. 3-5). These observations signify that more continuous sedimentation existed elsewhere in the region across the onset of OAE2 compared to the GSSP locality and, further, they constrain the duration of the hiatus at the GSSP section to 59±10 kyr (Fig. 5). Summing the quantified hiatuses above LS5 and at the base of OAE2, we estimate that the GSSP section is missing 82±10 kiloyears in detectable hiatal surfaces (i.e., hiatuses of ≥10s kiloyears in duration). This suggests that the GSSP section preserves ~90% of the temporal duration of the broader OAE2 interval from the Os_i excursion to CIE termination.

Although the GSSP section is conformable spanning the Cenomanian-Turonian stage boundary, adhering to criteria for GSSPs, the hiatus at the onset of OAE2 in this site omits a brief time interval. This interval, however, is represented in other sections within the basin that can be readily correlated to the GSSP site, such as the Angus and SH#1 cores.

OAE2 Time Scale Comparisons

Oceanic Anoxic Event 2, which was first identified as a black shale succession spanning the Cenomanian-Turonian boundary at many marine sites (Schlanger and Jenkyns, 1976; Arthur et al., 1987), can be recognized globally by a prominent positive carbon isotope excursion (CIE) (Scholle and Arthur, 1980). Defining OAE2 from the base of this CIE to a return to stable background $\delta^{13}C$ values at the top of the event (the "long" definition, as compared to the shorter "end of CIE plateau" definition: Tsikos et al., 2004; Sageman et al., 2006), recent studies from the Iona-1 Core in the Maverick Basin of Texas and in Gongzha, Tibet found comparatively expanded durations of OAE2 of 920±170 kyr and 820±25 kyr, respectively (Eldrett et al., 2015; Li et al., 2017). Compared to syntheses from the Western Interior Basin, these recent findings are equivalent in duration to the long definition values of 866±19 kyr (Sageman et al., 2006). However, to reconcile the nominal offsets in mean durations, authors have noted the occurrence of pre-cursor isotopic events in the Iona-1 Core of Texas and stratigraphic expansion in Tibet, proposing that hiatuses at the base of the OAE2 CIE in the central WIB sites account for the discrepancies (Eldrett et al., 2017; Li et al., 2017). With our new quantification of the hiatus at the base of the OAE2 CIE in the Portland Core and the addition of more continuous Os_i records in the Angus and SH#1 cores, it is possible to assess this hypothesis more critically. Additionally, a recent Os_i chemostratigraphy of the CTB succession in the Iona-1 Core (Sullivan et al., in press) provides another distinct profile to correlate and compare records from Utah and Colorado to Texas.

When the records from the central WIB and the Iona-1 cores are aligned and correlated using $\delta^{13}C$ and Os_i excursions, there is strong overlap between the floating eccentricity bandpass astronomical time scales of OAE2 (Fig. DR5). Bandpass filtering of the short eccentricity ($E_{2\text{-}3}$) spectral peak in both the central WIB (Meyers et al., 2001; Jones et al., 2019) and Texas (Eldrett et al., 2015) detect approximately six $E_{2\text{-}3}$ cycles from the CIE base to the top of the CIE plateau (i.e., short definition ~600 kyr) and seven to eight $E_{2\text{-}3}$ cycles from the CIE base to the return to stable $\delta^{13}C$ values (i.e. long definition) (Fig. 5). Most other sites with relatively conformable records of OAE2 globally preserve a similar number of cycles (see figure 9 of Charbonnier et al., 2018). However, discrepancies in timing of the CIE emerge when comparing the central WIB sites to the traced short obliquity cycle (O1: ~50 kyr) time scale for the Iona-1 Core preferred by Eldrett et al. (2015), which reports a longer duration for OAE2 (Fig. DR5). Thus, since eccentricity-based time scales correspond well among the sites, it is likely that the reported discrepancy between the Texas and central WIB durations for OAE2 primarily arises not from hiatuses, but from the usage of the less common O1 cycle to tune the Iona-1 Core record. This finding suggests that, despite the increased amplitude of obliquity forcing during the CTB (Meyers et al., 2012a; Charbonnier et al., 2018), the O1 cycle is less reliable for astronomical tuning of mid-Cretaceous stratigraphic datasets given markedly lower power in the La2004 and La2010 solutions than other astronomical terms (Laskar et al., 2004; Laskar et al., 2011; Wu et al., 2013). The hypothesis that minor offsets in durations of OAE2 records in the Eagle Ford, Tibet, and the central WIB originate from cyclostratigraphic techniques, as opposed to hiatuses or significant differences in local stratigraphic preservation of the event, is consistent with the presented finding of a relatively short-lived hiatus at the base of the OAE2 CIE in the Portland Core and GSSP locality.

In addition, the Eagle Ford record from the Iona-1 Core preserves two ~+1-2‰ $\delta^{13}C$ excursions underlying the main body of OAE2 (Fig. 5) labelled as pre-cursor isotope events (PCEs). These PCE do not appear in the Portland Core $\delta^{13}C$ record, a feature that has been attributed to hiatuses in the central WIB (Eldrett et al., 2015; 2017). However, the Os_i excursion of OAE2 occurs below the PCEs in the Iona-1 Core (Sullivan et al., in press). When compared to the Os_i records of the central WIB, this chemostratigraphic relationship indicates another possibility: that the PCEs in the Iona-1 Core correspond to the "A" $\delta^{13}C$ peak for OAE2 of Pratt (1985) in the central WIB. The position of biostratigraphic markers in the last occurrence (LO) datums of the foraminifera *Rotalipora cushmani* and nannofossil marker *Axopodorhabdus albianus*, as well as equivalent durations for OAE2 from eccentricity bandpasses, support this scenario (Fig. 5). The Iona-1 Core may preserve two $\delta^{13}C$ peaks within the "A" interval due to a more stratigraphically expanded record compared to the Portland Core and Pueblo GSSP. Nonetheless, additional high-resolution $\delta^{13}C$ chemostratigraphic studies of the onset of OAE2 in the WIB, such as in the conformable Angus Core (Fig. 3), are needed to further test the hypothesis that the PCEs correlate to the "A" CIE peak.

Radioisotope Geochronology of the Cenomanian-Turonian Boundary

The five new $^{40}Ar/^{39}Ar$ ages (Fig. 7) for bentonites B, C, and D from Nipple Creek, UT, Lohali Point, Arizona, and Pueblo, Colorado all overlap with recent $^{40}Ar/^{39}Ar$ ages from the WIB (Meyers et al., 2012b; Jicha et al., 2016). The new $^{40}Ar/^{39}Ar$ age for Bentonite B at Nipple Creek (NC-B) is also equivalent within uncertainty to the youngest zircon U-Pb data of the bentonite (Barker et al., 2011; Meyers et al., 2012b), indicating that these two radioisotopic chronometers are synchronized. The new age of Bentonite D from Nipple Creek (NC-D) overlaps within total temporal uncertainty of the $^{40}Ar/^{39}Ar$ age of Meyers et al. (2012b), but does not overlap with the other new age for Bentonite D at Lohali Point, Arizona (90-O-34) (Table 2). Its mean $^{40}Ar/^{39}Ar$ age is 230 kyr younger than the mean age from Meyers et al. (2012b) and 357 kyr younger than the ash at Lohali Point (Fig. 7). Thus, the NC-D date represents an outlier and we exclude it from calculations of the age of the CTB.

When anchored to the short eccentricity traced floating astronomical time scale for the Portland Core (Meyers et al., 2001), the new $^{40}Ar/^{39}Ar$ dates for bentonites B (NC-B), C (NC-C, K-07-01C), and D (90-O-34-D) produce numerical age estimates for the Cenomanian-Turonian boundary (Table 2, Table DR1 in Data Repository). The 2σ uncertainties on individual CTB age estimates derive from the full radioisotopic, stage boundary placement (±25 kyr), and astrochronologic (±25 kyr) sources of uncertainty combined in quadrature (*sensu* Sageman et al., 2014b). The weighted mean age and 2σ uncertainty for the CTB from all four anchoring scenarios for new dates is 94.05±0.08 Ma. If we include all recent $^{40}Ar/^{39}Ar$ dates for these bentonites and U-Pb dates that do not exhibit evidence for inheritance (Barker et al., 2011; Meyers et al., 2012b; Eldrett et al., 2015; Jicha et al., 2016), the weighted mean CTB age is 93.95±0.05 Ma. The CTB age estimate from the four new $^{40}Ar/^{39}Ar$ dates of this study is within uncertainty of recent radioisotopically calibrated ages reported for the boundary (Barker et al., 2011; Meyers et al., 2012b; Eldrett et al., 2015). However, the weighted mean age options proposed for the CTB from the new bentonite dates and from the compilation of new and recent dates (Fig. 7) are nominally older than the Meyers et al. (2012) age used for the CTB in the Geologic Time Scale (GTS) 2012 (Ogg and Hinnov, 2012) by 150 kyr and 50 kyr, respectively.

Although the new radioisotopically anchored and astronomically tuned age estimate for the CTB from southern Utah is consistent with existing geochronologic records, the onset age for OAE2 differs with the record from Texas. The U-Pb anchored astronomical time scale from the Iona-1 Core in the Eagle Ford of Texas places the age of the base of OAE2 ~300 kyr older (94.8-94.9 Ma) (Eldrett et al., 2015; Eldrett et al., 2017) than the records of the central WIB (94.55±0.16 Ma) (this study) and the Yezo Group, Japan (Du Vivier et al., 2015b). Several studies spanning a wide range of ages demonstrate that the astronomical calibration of the FCs standard at 28.201 Ma (Kuiper et al., 2008) yields $^{40}Ar/^{39}Ar$ dates that are indistinguishable from, or slightly younger than, CA-ID-TIMS (chemical abrasion-isotope dilution thermal ionization mass spectrometry) U-Pb dates from zircons in the same, or correlative, rocks (e.g., Meyers et al., 2012b; Rivera et al., 2014; Sageman et al., 2014b; Singer et al., 2014; Andersen et al., 2017). This is true unless the U-Pb zircon dates show clear patterns of inheritance (e.g., Wotzlaw et al., 2013) as is the case for 8 of the 10 ash beds for which Eldrett et al. (2015) report U-Pb dates. It is thus unlikely that the disagreement between our new date for the onset of OAE2 from the central WIB and the U-Pb age reported by Eldrett et al. (2015) in the Iona-1 Core reflect miscalibration of the $^{40}Ar/^{39}Ar$ chronometer. Rather, we suspect that pre-eruptive zircon crystallization or inheritance biases most of the U-Pb dates from the Eagle Ford to older ages, as several ash beds appear anomalously old and do not obey stratigraphic superposition (Eldrett et al., 2015). Meyers et al. (2012b) also previously noted inherited zircons based on U-Pb dating of several bentonites in the central WIB. Alternatively, this offset between the proposed initiation ages for OAE2 may result from the use of the O1 cycle for tuning the age-depth model in the Eagle Ford, as discussed above.

Eustatic Lowstand Preceding OAE2

Spatial variability in the development of hiatuses locally in the WIB underscores an undulating nature to bathymetry of the epeiric seaway, even within the same structural zones of the basin, such as the "axial basin." Modern shallow marine foreland basins, such as the Persian Gulf Basin, exhibit analogous local variation in bathymetry linked to long-lived geologic structures (Kassler, 1973). Similarly, we posit that some deformation of the Rock Canyon Anticline could have occurred during the Cretaceous and contributed to local shoaling, exposing the bathymetric high to wave base mixing and winnowing during sea level lowstands.

The basal OAE2 hiatus at the GSSP locality and Portland Core occurs within the uppermost ammonite *Metoicoceras mosbyense* Biozone, and has previously been interpreted to represent a minor lowstand in the WIB (Sageman, 1985; Arthur and Sageman, 2005; Gale et al., 2008). Along the western margin of the basin in southern Utah, the shoreline progrades ~150 km east ("S1" genetic sequence in Fig. 2) and a regression incises ~10 m of strata below the OAE2 CIE at some sites (Uličný, 1999; Laurin et al., 2019). Therefore, the basal OAE2 hiatus at the Pueblo GSSP locality and Portland Core may represent Late Cenomanian winnowing of a bathymetric high during a minor lowstand in the basin. Similarly, intervals of the middle Hartland Shale contain thin beds of winnowed skeletal limestones that correlate shoreward to a clastic wedge, suggesting another lowstand (Sageman, 1985, 1996). Bone beds, such as the one reported from the basal OAE2 hiatal surface at the Pueblo GSSP locality (Eicher and Diner, 1989), commonly correspond to transgressive surfaces in sequence stratigraphic models of epeiric seaways (Brett, 1995). Thus, the thin bone bed at the GSSP locality could instead represent a condensed bed that correlates to sediment starvation during the transgression overlying genetic sequence S1 of Utah (equivalent to Unit 6B of Uličný, 1999). Regardless of whether the hiatus corresponds directly to winnowing during relative sea level fall or condensation from the immediately subsequent transgression, the pre-OAE2 hiatus and shoreline trajectories in the WIB are reasonably interpretable as associated with a lowstand sequence boundary.

Moreover, a compilation of global relative sea level records, constrained by ammonite biostratigraphy and/or $\delta^{13}C$ chemostratigraphy, reveals coeval sequence boundaries and lowstands underlying OAE2 at many localities, including: the English Chalk (Gale et al., 1993), the Paris Basin (Robaszynski et al., 1998), Germany (Voigt et al., 2006; Richardt et al., 2013), Czech Republic (Uličný et al., 1997), Peru (Navarro-Ramirez et al., 2016), Mexico (Elrick et al., 2009), southern New Mexico (Mack et al., 2016), the northern Gulf of Mexico (Lowery et al., 2017), Jordan (Wendler et al., 2014), Lebanon (Grosheny et al., 2017), Israel (Buchbinder et al., 2000), Egypt (Nagm et al., 2014), and Morocco (Kuhnt et al., 2009). Consistency among these global Upper Cretaceous relative sea level records ties the hiatus in the uppermost Hartland Shale in the WIB to an apparent eustatic lowstand preceding the onset of OAE2, coeval with or just preceding a major pulse of LIP volcanism (Fig. 8). The link between LIP initiation and eustatic lowstand is consistent with original hypotheses of volcano-tectono-eustatic feedbacks at the onset of OAE2, followed by eustatic transgression with expanded shelfal area and organic carbon deposition (Arthur et al., 1987). However, eccentricity pacing of relative sea level through the event along the western margin of the seaway indicates at least a partial background control from climatic processes as well (Jones et al., 2019; Laurin et al., 2019).

Refined Timing of LIP Volcanism and the OAE2 Carbon Cycle Perturbation

The apparently conformable Os_i chemostratigraphy from the Angus Core, with its high-resolution astronomical and radioisotopic time scale, provides a refined timeline of LIP volcanic activity in relation to the carbon cycle perturbation at the onset of OAE2 (Figs. 5, 8). Globally, all Os_i records of OAE2, including from the WIB, exhibit a geologically rapid increase in the flux of hydrothermal/volcanic osmium to the marine realm (Turgeon and Creaser, 2008; Du Vivier et al., 2014; Du Vivier et al., 2015b; Schröder-Adams et al., 2019; Sullivan et al., in press). In the case of the astronomically tuned record from the Angus Core, the precipitous unradiogenic Os_i excursion occurs abruptly in less than 20 kiloyears beginning 60 kiloyears before the CIE, with a subtle decrease in Os_i preceding the main Os_i excursion, 80-100 kiloyears before the CIE (Figs. 2, 5, 8). Assuming that a massive increase in the hydrothermal/mantle C flux coincided with this rapid hydrothermal Os pulse (e.g., Kuroda et al., 2007), carbon release to the ocean-atmosphere system on this time scale would have occurred rapidly enough to potentially alter marine carbonate chemistry (Du Vivier et al., 2015a) (Fig. 8).

The positive carbon isotope excursion marking the onset of OAE2 occurred only after a significant temporal lag following the abrupt onset of LIP volcanism, on the order of 10s of kiloyears. This study quantifies that lag at 59±10 kiloyears using the astronomical time scale for the Angus Core (see Results, Figs. 4-5, 8), a similar, though slightly longer duration than previous estimates (Turgeon and Creaser, 2008; Du Vivier et al., 2015a). Fundamentally, this lag represents the time between (1) the onset of massive submarine LIP volcanism, CO_2 degassing, and delivery of reduced metals to the marine realm; and (2) the carbon cycle perturbation of OAE2 recorded in $\delta^{13}C$ records, which ultimately reflects the spread in areal extent of anoxic and sulfidic marine bottom waters and burial/preservation of organic carbon (Scholle and Arthur, 1980; Owens et al., 2013).

The duration of the lag exceeds interpreted oceanic mixing time scales by an order of magnitude and, therefore, cannot solely represent the time needed to circulate water masses rich with biolimiting nutrients derived from submarine volcanic or continentally weathered sources, even in a sluggish mid-Cretaceous ocean (e.g., Turgeon and Creaser, 2008). It is possible that osmium cycle proxies (i.e., Os_i) are more sensitive to submarine LIP volcanism than carbon cycle proxies, and we have overestimated the pace of LIP CO_2 outgassing; tens of kiloyears could have been needed to accumulate CO_2 in the atmosphere. However, OAE2 preserves one of the longest-lived and most abruptly initiated unradiogenic Os_i excursions known from the Phanerozoic, suggesting a rapidly initiated and long-lived episode of prolific volcanism.

Alternatively, circulation of the marine dissolved oxygen reservoir typically provides a buffer against the prolonged expansion of anoxic bottom waters and organic carbon burial exhibited during OAEs. The inertia between volcanic CO_2 input and widespread anoxia/carbon burial likely represents the globally-averaged drawdown of this substantial marine oxygen reservoir during OAE2. Accordingly, the presented duration of the Os-C lag is equivalent to the duration of a gradual drawdown of redox sensitive trace metals and bottom water oxygen levels at

Demerara Rise (tropical Atlantic) which precedes OAE2 (Hetzel et al., 2009; Ostrander et al., 2017). The subsequent global-net enhanced burial and accumulation of organic carbon only drove the OAE2 CIE following this 10's of kyr deoxygenation process (Fig. 8). This implies that the preservation of organic carbon due to anoxic/euxinic bottom and pore waters, mediated by organic matter sulfurization (Raven et al., 2018), was a key paleoceanographic feedback that ultimately triggered the OAE2 CIE (Mort et al., 2007), perhaps more so than the initial increases in marine primary productivity.

Multiple Volcanic Pulses

In addition to a volcanic pulse preceding OAE2, ^{192}Os concentrations increase in the interval underlying Bentonite A, consistent with a second episode of submarine volcanism (Table 1; Figs. 3-4). In this interval within the upper half of the Os_i excursion in the WIB, already unradiogenic Os_i values at each site decrease further, subtly but consistently, and by more than analytical uncertainty. Values of Os_i decrease in the SH#1, Angus, and Portland cores respectively by 0.066, 0.026, and 0.053 below Bentonite A (Table 1; Figs. 3-5). Thus, the WIB osmium chemostratigraphy indicates that the LIP emanated at least two pulses of volcanic activity that punctuated an elevated background rate of volcanism spanning the onset and the early interval of OAE2 (Fig. 8). Similar scenarios of multiple pulses of volcanism (Sullivan et al., in press) and anoxia (Jenkyns et al., 2017; Clarkson et al., 2018) during the event have been reported, hinting at links between the intensity of volcanism and marine deoxygenation, although correlations appear to exhibit offsets in the precise timing of these processes.

Re-Os Geochemical Dynamics in an Epeiric Seaway

The proximal-distal transect of the mid-latitudes of the WIB constrains spatial variability of Os_i chemostratigraphic records in a shallow continental seaway through a period of massive volcanism and eustatic transgression. Osmium chemostratigraphy of both Quaternary and Cenomanian-Turonian records exhibit a degree of spatial variability in Os_i composition among oceanic basins, highlighting the sensitivity of a given locality's record to water mass heterogeneity and the proximity of weathered sources of osmium (Du Vivier et al., 2014; Du Vivier et al., 2015b; Rooney et al., 2016). Despite fluctuating sea level in the WIS and likely some degree of basin restriction, the unradiogenic Os_i excursion and enrichment in ^{192}Os at the onset of OAE2 is robustly preserved in each of the three sites transecting the depositional settings in the basin, heralding a pulse of LIP volcanism (Fig. 5).

Values of Os_i are equivalent across the basin during the syn- and post-OAE2 intervals, including at the most proximal locality - SH#1 (Fig. 6). However, Os_i values in the SH#1 Core are highly radiogenic prior to OAE2 compared to sites in the axial basin, at a time when the shoreline of the western margin of the seaway was closer to the site (~35 km, cf. Laurin and Sageman, 2007). The radiogenic values in this interval reflect the proximity of continentally weathered Os sources in the Sevier Belt. It appears that when the shoreline was within 10's of kilometers of the site, the Os_i proxy was sensitive to runoff from the Sevier Belt, whereas when the shoreline was more than ~100 km away, the proxy tracked values of Os_i that characterize the broader seaway and pelagic marine records. Nonetheless, the pre-OAE2 interval at SH#1 exhibits a shift to unradiogenic values below the major Os_i excursion (Fig. 3), similar to records globally (Du Vivier et al., 2014; Du Vivier et al., 2015b). These findings indicate that the proxy remains sensitive to major changes in the global fluxes of the marine Os cycle in proximal marine settings during LIP episodes, despite offsets in the absolute values of Os_i trends.

CONCLUSION

Our new chemostratigraphic compilation from the Angus and SH#1 cores spans the onset of OAE2 in the WIB. The proximal-distal transect defines spatial variability and local controls on the Re-Os proxy for volcanism in a semi-restricted epeiric seaway. Observations support prolific LIP volcanic activity in the Late Cenomanian, most likely in the Caribbean and Arctic regions. Notably, the characteristic unradiogenic Os_i chemostratigraphic marker of volcanism preceding OAE2 extends to SH#1, the most proximal setting studied in the WIB.

New $^{40}Ar/^{39}Ar$ dates for traceable bentonites in the WIB, combined with recently published radioisotopic analyses, yield an astronomically calibrated age for the Cenomanian-Turonian stage boundary of 93.95±0.05 (2σ) Ma, which is consistent with other recent age estimates but slightly older than the GTS 2012 age. The integrated radioisotope geochronology, astrochronology, chemostratigraphy, and biostratigraphy from the WIB provide a high-resolution age model refining the chronology of triggers and paleoenvironmental feedbacks for OAE2. Most notably, a 59±10 kyr lag between intensification of LIP volcanism and widespread, globally-averaged organic carbon burial is quantified at the onset of OAE2. This lag during the initial phase of volcanism suggests net-deoxygenation of the global ocean over tens of kiloyears, past a threshold for widespread organic C preservation, was a critical process in the ultimate initiation of OAE2. Further, the rapid onset of LIP volcanism preceding OAE2 is consistent with a scenario of increased pCO_2, altered marine carbonate chemistry, and decreased aragonite/calcite saturation levels in the global ocean (Du Vivier et al., 2015a). Additionally, a second pulse of LIP volcanism ~100 kyr after the onset of the CIE is consistent with earlier investigations.

The refined chronostratigraphic framework is also used to assess stratigraphic conformability and correlation of reference sites for the CTB in the WIB. The duration of a hiatus in the crucial onset interval of OAE2 at Pueblo, CO (Base Turonian GSSP) and the Portland Core is equivalent to the geologically brief temporal lag between volcanism and carbon cycle perturbation. This hiatus is associated with a minor eustatic lowstand and subsequent transgression preceding OAE2, recorded in many shallow marine settings globally, which is potentially linked to tectonic or climatic feedbacks from the coeval initiation of LIP volcanism. Based on Os_i chemostratigraphic correlation, minor $\delta^{13}C$ excursions underlying the main OAE2 CIE in the Eagle Ford of Texas appear to correspond to the "A" segment of the $\delta^{13}C$ record in the central WIB. Additionally, residual offsets in recent time scales for OAE2 may originate in part from biases in radioisotope geochronology, such as zircon inheritance, and/or differences in astrochronologic tuning methodologies and chemostratigraphic definitions of the event.

ACKNOWLEDGEMENTS

We thank: Antonia Hofmann, Geoff Nowell, and Chris Ottley for assistance with Re-Os geochemical analyses; Steve Meyers for providing the ATS for the Portland Core; Bryan Wathen for mineral separation; Rosie Oakes, R. Mark Leckie, Julio Sepulveda, Tim Bralower, Scott Karduck, and Amanda Parker for assistance logging and sampling the SH#1 Core; R. Mark Leckie, Jiří Laurin, and David Uličný for insightful discussions on the stratigraphy of the Kaiparowits Plateau; Brad Cramer and an anonymous referee for constructive reviews improving the quality of the manuscript; the USGS for drilling the SH#1 Core; and Encana for donating the Angus Core to Northwestern University. This article represents a portion of the doctoral research of MMJ at Northwestern University. BBS acknowledges funding from NSF Earth-Life Transitions grant

#1338312 and thanks the U.S. BLM for sample collection permit 9560 (UT-030). DS acknowledges funding from the TOTAL Endowment Fund and the Dida Scholarship.

REFERENCES CITED

Adams, D. D., Hurtgen, M. T., and Sageman, B. B., 2010, Volcanic triggering of a biogeochemical cascade during Oceanic Anoxic Event 2: Nature Geoscience, v. 3, no. 3, p. 201-204, https://doi:10.1038/ngeo743.

Andersen, N. L., Jicha, B. R., Singer, B. S., and Hildreth, W., 2017, Incremental heating of Bishop Tuff sanidine reveals preeruptive radiogenic Ar and rapid remobilization from cold storage: Proceedings of the National Academy of Sciences, v. 114, no. 47, p. 12407-12412, https://doi.org/10.1073/pnas.1709581114.

Arthur, M. A., and Sageman, B. B., 1994, Marine Black Shales: Depositional Mechanisms and Environments of Ancient Deposits: Annual Review of Earth and Planetary Sciences, v. 22, no. 1, p. 499-551, https://doi.org/10.1146/annurev.ea.22.050194.002435.

Arthur, M. A., and Sageman, B. B., 2005, Sea-level control on source-rock development: perspective from the Holocene Black Sea, the mid-Cretaceous Western Interior Basin of North America, and the Late Devonian Appalachian Basin, *in* Harris, N.B., ed., Deposition of Organic-Carbon-Rich Sediments: Models, Mechanisms, and Consequences: SEPM (Society for Sedimentary Geology) Special Publication v. 82: p. 35–59, https://doi.org/10.2110/pec.05.82.0035.

Arthur, M. A., Schlanger, S. O., and Jenkyns, H. C., 1987, The Cenomanian-Turonian Oceanic Anoxic Event, II. Palaeoceanographic controls on organic-matter production and preservation: Geological Society, London, Special Publications, v. 26, no. 1, p. 401-420, https://doi.org/10.1144/GSL.SP.1987.026.01.25.

Barclay, R. S., McElwain, J. C., and Sageman, B. B., 2010, Carbon sequestration activated by a volcanic CO2 pulse during Ocean Anoxic Event 2: Nature Geoscience, v. 3, no. 3, p. 205-208, https://doi.org/10.1038/ngeo757.

Baresel, B., Bucher, H., Bagherpour, B., Brosse, M., Guodun, K., and Schaltegger, U., 2017, Timing of global regression and microbial bloom linked with the Permian-Triassic boundary mass extinction: implications for driving mechanisms: Scientific Reports, v. 7, p. 43630, DOI: 10.1038/srep43630.

Barker, I. R., Moser, D. E., Kamo, S. L., and Plint, A. G., 2011, High-precision U–Pb zircon ID–TIMS dating of two regionally extensive bentonites: Cenomanian Stage, Western Canada Foreland Basin: Canadian Journal of Earth Sciences, v. 48, no. 2, p. 543-556, https://doi.org/10.1139/E10-042.

Bottini, C., Cohen, A. S., Erba, E., Jenkyns, H. C., and Coe, A. L., 2012, Osmium-isotope evidence for volcanism, weathering, and ocean mixing during the early Aptian OAE 1a: Geology, v. 40, no. 7, p. 583-586, https://doi.org/10.1130/G33140.1.

Bralower, T. J., 1988, Calcareous nannofossil biostratigraphy and assemblages of the Cenomanian-Turonian Boundary interval: implications for the origin and timing of oceanic anoxia: Paleoceanography, v. 3, no. 3, p. 275-316, https://doi.org/10.1029/PA003i003p00275.

Brett, C. E., 1995, Sequence Stratigraphy, Biostratigraphy, and Taphonomy in Shallow Marine Environments: PALAIOS, v. 10, no. 6, p. 597-616, http://dx.doi.org/10.2307/3515097.

Buchbinder, B., Benjamini, C., and Lipson-Benitah, S., 2000, Sequence development of Late Cenomanian-Turonian carbonate ramps, platforms and basins in Israel: Cretaceous Research, v. 21, no. 6, p. 813-843, https://doi.org/10.1006/cres.2000.0228.

Carpenter, K., 2014, Where the sea meets the land: the unresolved Dakota problem in Utah, *in* MacLean, J. S., Biek, R. F., and Huntoon, J. E., eds., Geology of Utah's Far South, Volume 43, Utah Geological Association, p. 357-372.

Charbonnier, G., Boulila, S., Spangenberg, J. E., Adatte, T., Föllmi, K. B., and Laskar, J., 2018, Obliquity pacing of the hydrological cycle during the Oceanic Anoxic Event 2: Earth and Planetary Science Letters, v. 499, p. 266-277, https://doi.org/10.1016/j.epsl.2018.07.029.

Clarkson, M. O., Stirling, C. H., Jenkyns, H. C., Dickson, A. J., Porcelli, D., Moy, C. M., Pogge von Strandmann, P. A. E., Cooke, I. R., and Lenton, T. M., 2018, Uranium isotope evidence for two episodes of deoxygenation during Oceanic Anoxic Event 2: Proceedings of the National Academy of Sciences, v. 115, no. 12, p. 2918-2923, www.pnas.org/cgi/doi/10.1073/pnas.1715278115.

Cobban, W. A., and Scott, G. R., 1972, Stratigraphy and ammonite fauna of the Graneros Shale and Greenhorn Limestone near Pueblo, Colorado: U.S. Geological Survey Professional Paper 645, 108 p., https://doi.org/10.3133/pp645.

Corbett, M. J., and Watkins, D. K., 2013, Calcareous nannofossil paleoecology of the mid-Cretaceous Western Interior Seaway and evidence of oligotrophic surface waters during OAE2: Palaeogeography, Palaeoclimatology, Palaeoecology, v. 392, p. 510-523, http://dx.doi.org/10.1016/j.palaeo.2013.10.007.

Du Vivier, A. D. C., Jacobson, A. D., Lehn, G. O., Selby, D., Hurtgen, M. T., and Sageman, B. B., 2015a, Ca isotope stratigraphy across the Cenomanian–Turonian OAE 2: Links between volcanism, seawater geochemistry, and the carbonate fractionation factor: Earth and Planetary Science Letters, v. 416, p. 121-131, http://dx.doi.org/10.1016/j.epsl.2015.02.001.

Du Vivier, A. D. C., Selby, D., Condon, D. J., Takashima, R., and Nishi, H., 2015b, Pacific Os-187/Os-188 isotope chemistry and U-Pb geochronology: Synchroneity of global Os isotope change across OAE 2: Earth and Planetary Science Letters, v. 428, p. 204-216, http://dx.doi.org/10.1016/j.epsl.2015.07.020.

Du Vivier, A. D. C., Selby, D., Sageman, B. B., Jarvis, I., Groecke, D. R., and Voigt, S., 2014, Marine Os-187/Os-188 isotope stratigraphy reveals the interaction of volcanism and ocean circulation during Oceanic Anoxic Event 2: Earth and Planetary Science Letters, v. 389, p. 23-33, http://dx.doi.org/10.1016/j.epsl.2013.12.024.

Eicher, D. L., and Diner, R., 1985, Foraminifera as Indicators of Water Mass in the Cretaceous Greenhorn Sea, Western Interior, *in* Pratt, L. M., Kauffman, E. G., and Zelt, F. B., eds., Fine-Grained Deposits and Biofacies of the Cretaceous Western Interior Seaway: Evidence of Cyclic Sedimentary Processes, SEPM Society for Sedimentary Geology, p. 60-71, https://doi.org/10.2110/sepmfg.04.060.

Eicher, D. L., and Diner, R., 1989, Origin of the cretaceous bridge creek cycles in the western interior, United States: Palaeogeography, Palaeoclimatology, Palaeoecology, v. 74, no. 1, p. 127-146, https://doi.org/10.1016/0031-0182(89)90023-0.

Eicher, D. L., and Worstell, P., 1970, Cenomanian and Turonian Foraminifera from the Great Plains, United States: Micropaleontology, v. 16, no. 3, p. 269-324, https://www.jstor.org/stable/1485079.

Elder, W. P., 1988, Geometry of Upper Cretaceous bentonite beds: Implications about volcanic source areas and paleowind patterns, western interior, United States: Geology, v. 16, no. 9, p. 835-838, https://doi.org/10.1130/0091-7613(1988)016%3C0835:GOUCBB%3E2.3.CO;2.

Elder, W. P., 1989, Molluscan extinction patterns across the Cenomanian-Turonian Stage boundary in the Western Interior of the United States: Paleobiology, v. 15, no. 3, p. 299-320, https://doi.org/10.1017/S0094837300009465.

Elder, W. P., 1991, Molluscan paleoecology and sedimentation patterns of the Cenomanian-Turonian extinction interval in the southern Colorado Plateau region, *in* Nations, J. D., and Eaton, J. G., eds., Stratigraphy, depositional environments, and sedimentary tectonics of the Western Margin, Cretaceous Western Interior Seaway, Volume 260, Geological Society of America Special Paper, p. 113-137, https://doi.org/10.1130/SPE260-p113.

Elder, W. P., Gustason, E. R., and Sageman, B. B., 1994, Correlation of basinal carbonate cycles to nearshore parasequences in the Late Cretaceous Greenhorn seaway, Western Interior U.S.A: Geological Society of America Bulletin, v. 106, no. 7, p. 892-902, https://doi.org/10.1130/0016-7606(1994)106%3C0892:COBCCT%3E2.3.CO;2.

Elder, W. P., and Kirkland, J. I., 1985, Stratigraphy and Depositional Environments of the Bridge Creek Limestone Member of the Greenhorn Limestone at Rock Canyon Anticline Near Pueblo, Colorado, *in* Pratt, L. M., Kauffman, E. G., and Zelt, F. B., eds., Fine-Grained Deposits and Biofacies of the Cretaceous Western Interior Seaway: Evidence of Cyclic Sedimentary Processes, SEPM Society for Sedimentary Geology, p.122-134, https://doi.org/10.2110/sepmfg.04.122.

Elderbak, K., and Leckie, R. M., 2016, Paleocirculation and foraminiferal assemblages of the Cenomanian–Turonian Bridge Creek Limestone bedding couplets: Productivity vs. dilution during OAE2: Cretaceous Research, v. 60, p. 52-77, https://doi.org/10.1016/j.cretres.2015.11.009.

Eldrett, J. S., Dodsworth, P., Bergman, S. C., Wright, M., and Minisini, D., 2017, Water-mass evolution in the Cretaceous Western Interior Seaway of North America and equatorial Atlantic: Climate of the Past, v. 13, no. 7, p. 855-878, https://doi.org/10.5194/cp-13-855-2017.

Eldrett, J. S., Ma, C., Bergman, S. C., Lutz, B., Gregory, F. J., Dodsworth, P., Phipps, M., Hardas, P., Minisini, D., Ozkan, A., Ramezani, J., Bowring, S. A., Kamo, S. L., Ferguson, K., Macaulay, C., and Kelly, A. E., 2015, An astronomically calibrated stratigraphy of the Cenomanian, Turonian and earliest Coniacian from the Cretaceous Western Interior Seaway, USA: Implications for global chronostratigraphy: Cretaceous Research, v. 56, p. 316-344, https://doi.org/10.1016/j.cretres.2015.04.010.

Elrick, M., Molina-Garza, R., Duncan, R., and Snow, L., 2009, C-isotope stratigraphy and paleoenvironmental changes across OAE2 (mid-Cretaceous) from shallow-water platform carbonates of southern Mexico: Earth and Planetary Science Letters, v. 277, no. 3, p. 295-306, https://doi.org/10.1016/j.epsl.2008.10.020.

Gale, A. S., Jenkyns, H. C., Kennedy, W. J., and Corfield, R. M., 1993, Chemostratigraphy versus biostratigraphy: data from around the Cenomanian–Turonian boundary: Journal of the Geological Society, v. 150, no. 1, p. 29-32, https://doi.org/10.1144/gsjgs.150.1.0029.

Gale, A. S., Voigt, S., Sageman, B. B., and Kennedy, W. J., 2008, Eustatic sea-level record for the Cenomanian (Late Cretaceous)-Extension to the Western Interior Basin, USA: Geology, v. 36, no. 11, p. 859-862, https://doi.org/10.1130/G24838A.1.

Grosheny, D., Ferry, S., Lecuyer, C., Merran, Y., Mroueh, M., and Granier, B., 2017, The Cenomanian-Turonian Boundary Event (CTBE) in northern Lebanon as compared to regional data – Another set of evidences supporting a short-lived tectonic pulse coincidental with the event?: Palaeogeography, Palaeoclimatology, Palaeoecology, v. 487, p. 447-461, https://doi.org/10.1016/j.palaeo.2017.09.031.

Hattin, D. E., 1971, Widespread, synchronously deposited, burrow-mottled limestone beds in Greenhorn limestone (upper Cretaceous) of Kansas and southeastern Colorado: AAPG Bulletin, v. 55, no. 3, p. 412-431, https://doi.org/10.1306/5D25CF65-16C1-11D7-8645000102C1865D.

Hetzel, A., Boettcher, M. E., Wortmann, U. G., and Brumsack, H.-J., 2009, Paleo-redox conditions during OAE 2 reflected in Demerara Rise sediment geochemistry (ODP Leg 207): Palaeogeography Palaeoclimatology Palaeoecology, v. 273, no. 3-4, p. 302-328, https://doi.org/10.1016/j.palaeo.2008.11.005.

Holland, S. M., and Patzkowsky, M. E., 2015, The stratigraphy of mass extinction: Palaeontology, v. 58, no. 5, p. 903-924, https://doi.org/10.1111/pala.12188.

Jenkyns, H. C., Dickson, A. J., Ruhl, M., and van den Boorn, S. H. J. M., 2017, Basalt-seawater interaction, the Plenus Cold Event, enhanced weathering and geochemical change: deconstructing Oceanic Anoxic Event 2 (Cenomanian–Turonian, Late Cretaceous): Sedimentology, v. 64, no. 1, p. 16-43, https://doi.org/10.1111/sed.12305.

Jicha, B. R., Singer, B. S., and Sobol, P., 2016, Re-evaluation of the ages of 40Ar/39Ar sanidine standards and supereruptions in the western U.S. using a Noblesse multi-collector mass spectrometer: Chemical Geology, v. 431, p. 54-66, https://doi.org/10.1016/j.chemgeo.2016.03.024.

Jones, M. M., Sageman, B. B., Oakes, R. L., Parker, A. L., Leckie, R. M., Bralower, T. J., Sepúlveda, J., and Fortiz, V., 2019, Astronomical pacing of relative sea level during

Oceanic Anoxic Event 2: Preliminary studies of the expanded SH#1 Core, Utah, USA: GSA Bulletin, v. 131, no. 9-10, p. 1702-1722, https://doi.org/10.1130/B32057.1.

Joo, Y. J., and Sageman, B. B., 2014, Cenomanian to Campanian carbon isotope chemostratigraphy from the Western Interior Basin, USA: Journal of Sedimentary Research, v. 84, no. 7, p. 529-542, https://doi.org/10.2110/jsr.2014.38.

Kassler, P., 1973, The Structural and Geomorphic Evolution of the Persian Gulf, *in* Purser, B. H., ed., The Persian Gulf: Holocene Carbonate Sedimentation and Diagenesis in a Shallow Epicontinental Sea: Berlin, Heidelberg, Springer-Verlag, p. 10-32, https://doi.org/10.1007/978-3-642-65545-6_2.

Kauffman, E. G., 1977, Geological and biological overview: Western Interior Cretaceous Basin: The Mountain Geologist, v. 13, p. 75-99.

Kauffman, E. G., 1984, Paleobiogeography and evolutionary response dynamic in the Cretaceous Western Interior Seaway of North America, *in* Westermann, G. E. G., ed., Jurassic-Cretaceous Biochronology and Paleogeography of North America, Geological Association of Canada.

Kauffman, E. G., and Caldwell, W. G. E., 1993, The Western Interior Basin in space and time, *in* Caldwell, W. G. E., and Kauffman, E. G., eds., Evolution of the Western Interior Basin, Volume Special Paper 39, Geological Association of Canada, p. 1-30.

Kauffman, E. G., Sageman, B. B., Kirkland, J. I., Elder, W. P., Harries, P. J., and Villamil, T., 1993, Molluscan Biostratigraphy of the Cretaceous Western Interior Basin, North America, *in* Caldwell, W. G. E., and Kauffman, E. G., eds., Evolution of the Western Interior Basin, Volume 39, Geological Association of Canada, p. 397-434.

Kennedy, W. J., Walaszczyk, I., and Cobban, W. A., 2005, The global boundary stratotype section and point for the base of the Turonian stage of the cretaceous: Pueblo, Colorado, USA: Episodes, v. 28, no. 2, p. 93-104.

Kerr, A. C., 1998, Oceanic plateau formation: a cause of mass extinction and black shale deposition around the Cenomanian-Turonian boundary?: Journal of the Geological Society, v. 155, p. 619-626, https://doi.org/10.1144/gsjgs.155.4.0619.

Kidder, D. L., and Worsley, T. R., 2010, Phanerozoic Large Igneous Provinces (LIPs), HEATT (Haline Euxinic Acidic Thermal Transgression) episodes, and mass extinctions: Palaeogeography Palaeoclimatology Palaeoecology, v. 295, no. 1-2, p. 162-191, https://doi.org/10.1016/j.palaeo.2010.05.036.

Kuhnt, W., Holbourn, A., Gale, A., Chellai, E. H., and Kennedy, W. J., 2009, Cenomanian sequence stratigraphy and sea-level fluctuations in the Tarfaya Basin (SW Morocco): Geological Society of America Bulletin, v. 121, no. 11-12, p. 1695-1710, https://doi.org/10.1130/B26418.1.

Kuiper, K. F., Deino, A., Hilgen, F. J., Krijgsman, W., Renne, P. R., and Wijbrans, J. R., 2008, Synchronizing Rock Clocks of Earth History: Science, v. 320, no. 5875, p. 500-504, DOI: 10.1126/science.1154339.

Kuroda, J., Hori, R. S., Suzuki, K., Gröcke, D. R., and Ohkouchi, N., 2010, Marine osmium isotope record across the Triassic-Jurassic boundary from a Pacific pelagic site: Geology, v. 38, no. 12, p. 1095-1098, https://doi.org/10.1130/G31223.1.

Kuroda, J., Ogawa, N. O., Tanimizu, M., Coffin, M. F., Tokuyama, H., Kitazato, H., and Ohkouchi, N., 2007, Contemporaneous massive subaerial volcanism and late cretaceous

Oceanic Anoxic Event 2: Earth and Planetary Science Letters, v. 256, no. 1-2, p. 211-223, https://doi.org/10.1016/j.epsl.2007.01.027.

Laskar, J., Fienga, A., Gastineau, M., and Manche, H., 2011, La2010: a new orbital solution for the long-term motion of the Earth: Astronomy & Astrophysics, v. 532, http://dx.doi.org/10.1051/0004-6361/201116836.

Laskar, J., Robutel, P., Joutel, F., Gastineau, M., Correia, A. C. M., and Levrard, B., 2004, A long-term numerical solution for the insolation quantities of the Earth: Astronomy & Astrophysics, v. 428, no. 1, p. 261-285, https://doi.org/10.1051/0004-6361:20041335.

Laurin, J., Barclay, R. S., Sageman, B. B., Dawson, R. R., Pagani, M., Schmitz, M., Eaton, J., McInerney, F. A., and McElwain, J. C., 2019, Terrestrial and marginal-marine record of the mid-Cretaceous Oceanic Anoxic Event 2 (OAE 2): High-resolution framework, carbon isotopes, CO2 and sea-level change: Palaeogeography, Palaeoclimatology, Palaeoecology, v. 524, p. 118-136, https://doi.org/10.1016/j.palaeo.2019.03.019.

Laurin, J., and Sageman, B. B., 2007, Cenomanian-Turonian coastal record in SW Utah, USA: Orbital-scale transgressive-regressive events during Oceanic Anoxic Event II: Journal of Sedimentary Research, v. 77, no. 9-10, p. 731-756, https://doi.org/10.2110/jsr.2007.076.

Leckie, R. M., 1985, Foraminifera of the Cenomanian-Turonian Boundary Interval, Greenhorn Formation, Rock Canyon Anticline, Pueblo, Colorado, *in* Pratt, L. M., Kauffman, E. G., and Zelt, F. B., eds., Fine-Grained Deposits and Biofacies of the Cretaceous Western Interior Seaway: Evidence of Cyclic Sedimentary Processes, SEPM Society for Sedimentary Geology, p. 139-149, https://doi.org/10.2110/sepmfg.04.139.

Leithold, E. L., 1994, Stratigraphical architecture at the muddy margin of the Cretaceous Western Interior Seaway, southern Utah: Sedimentology, v. 41, no. 3, p. 521-542, https://doi.org/10.1111/j.1365-3091.1994.tb02009.x.

Li, Y.-X., Montañez, I. P., Liu, Z., and Ma, L., 2017, Astronomical constraints on global carbon-cycle perturbation during Oceanic Anoxic Event 2 (OAE2): Earth and Planetary Science Letters, v. 462, p. 35-46, https://doi.org/10.1016/j.epsl.2017.01.007.

Lowery, C. M., Cunningham, R., Barrie, C. D., Bralower, T., and Snedden, J. W., 2017, The Northern Gulf of Mexico During OAE2 and the Relationship Between Water Depth and Black Shale Development: Paleoceanography, v. 32, no. 12, p. 1316-1335, https://doi.org/10.1002/2017PA003180.

Ma, C., Meyers, S. R., Sageman, B. B., Singer, B. S., and Jicha, B. R., 2014, Testing the astronomical time scale for oceanic anoxic event 2, and its extension into Cenomanian strata of the Western Interior Basin (USA): Geological Society of America Bulletin, v. 126, no. 7-8, p. 974-989, https://doi.org/10.1130/B30922.1.

Mack, G. H., Hook, S., Giles, K. A., and Cobban, W. A., 2016, Sequence stratigraphy of the Mancos Shale, lower Tres Hermanos Formation, and coeval middle Cenomanian to middle Turonian strata, southern New Mexico, USA: Sedimentology, v. 63, no. 4, p. 781-808, https://doi.org/10.1111/sed.12238.

Meyers, S.R., Sageman, B.B., and Hinnov, L.A., 2001, Integrated quantitative stratigraphy of the Cenomanian- Turonian Bridge Creek Limestone member using evolutive harmonic analysis and stratigraphic modeling: Journal of Sedimentary Research, v. 71, no. 4, p. 628–644, http://dx.doi.org/10.1306/012401710628.

Meyers, S. R., and Sageman, B. B., 2004, Detection, quantification, and significance of hiatuses in pelagic and hemipelagic strata: Earth and Planetary Science Letters, v. 224, no. 1-2, p. 55-72, https://doi.org/10.1016/j.epsl.2004.05.003.

Meyers, S. R., Sageman, B. B., and Arthur, M. A., 2012a, Obliquity forcing of organic matter accumulation during Oceanic Anoxic Event 2: Paleoceanography, v. 27, https://doi.org/10.1029/2012PA002286.

Meyers, S. R., Sageman, B. B., and Hinnov, L. A., 2001, Integrated quantitative stratigraphy of the Cenomanian-Turonian bridge creek limestone member using evolutive harmonic analysis and stratigraphic modeling: Journal of Sedimentary Research, v. 71, no. 4, p. 628-644, https://doi.org/10.1306/012401710628.

Meyers, S. R., Siewert, S. E., Singer, B. S., Sageman, B. B., Condon, D. J., Obradovich, J. D., Jicha, B. R., and Sawyer, D. A., 2012b, Intercalibration of radioisotopic and astrochronologic time scales for the Cenomanian-Turonian boundary interval, Western Interior Basin, USA: Geology, v. 40, no. 1, p. 7-10, https://doi.org/10.1130/G32261.1.

Min, K., Mundil, R., Renne, P. R., and Ludwig, K. R., 2000, A test for systematic errors in 40Ar/39Ar geochronology through comparison with U/Pb analysis of a 1.1-Ga rhyolite: Geochimica et Cosmochimica Acta, v. 64, no. 1, p. 73-98, https://doi.org/10.1016/S0016-7037(99)00204-5.

Mort, H. P., Adatte, T., Foellmi, K. B., Keller, G., Steinmann, P., Matera, V., Berner, Z., and Stueben, D., 2007, Phosphorus and the roles of productivity and nutrient recycling during oceanic anoxic event 2: Geology, v. 35, no. 6, p. 483-486, https://doi.org/10.1130/G23475A.1.

Nagm, E., El-Qot, G., and Wilmsen, M., 2014, Stable-isotope stratigraphy of the Cenomanian–Turonian (Upper Cretaceous) boundary event (CTBE) in Wadi Qena, Eastern Desert, Egypt: Journal of African Earth Sciences, v. 100, p. 524-531, https://doi.org/10.1016/j.jafrearsci.2014.07.023.

Navarro-Ramirez, J. P., Bodin, S., and Immenhauser, A., 2016, Ongoing Cenomanian — Turonian heterozoan carbonate production in the neritic settings of Peru: Sedimentary Geology, v. 331, p. 78-93, https://doi.org/10.1016/j.sedgeo.2015.10.011.

Obradovich, J. D., 1993, A Cretaceous Time Scale, *in* Caldwell, W. G. E., and Kauffman, E. G., eds., Evolution of the Western Interior Basin, Volume Special Paper 39, Geological Association of Canada, p. 379-396.

Ogg, J.G., and Hinnov, L.A., 2012, Chapter 27, Cretaceous, The Geologic Time Scale: Boston, Elsevier, p.793-853, https://doi.org/10.1016/B978-0-444-59425-9.00027-5

Ostrander, C. M., Owens, J. D., and Nielsen, S. G., 2017, Constraining the rate of oceanic deoxygenation leading up to a Cretaceous Oceanic Anoxic Event (OAE-2: ~94 Ma): Science Advances, v. 3, no. 8, DOI: 10.1126/sciadv.1701020.

Owens, J. D., Gill, B. C., Jenkyns, H. C., Bates, S. M., Severmann, S., Kuypers, M. M. M., Woodfine, R. G., and Lyons, T. W., 2013, Sulfur isotopes track the global extent and dynamics of euxinia during Cretaceous Oceanic Anoxic Event 2: Proceedings of the National Academy of Sciences of the United States of America, v. 110, no. 46, p. 18407-18412, https://doi.org/10.1073/pnas.1305304110.

Oxburgh, R., 2001, Residence time of osmium in the oceans: Geochemistry, Geophysics, Geosystems, v. 2, no. 6, https://doi.org/10.1029/2000GC000104.

Percival, L. M. E., Jenkyns, H. C., Mather, T. A., Dickson, A. J., Batenburg, S. J., Ruhl, M., Hesselbo, S. P., Barclay, R., Jarvis, I., Robinson, S. A., and Woelders, L., 2018, Does large igneous province volcanism always perturb the mercury cycle? Comparing the records of Oceanic Anoxic Event 2 and the end-Cretaceous to other Mesozoic events: American Journal of Science, v. 318, no. 8, p. 799-860, doi: 10.2475/08.2018.01.

Peterson, F., 1969, Cretaceous sedimentation and tectonism in the southeastern Kaiparowits region, Utah, U.S. Geological Survey, Open-File Report 69-202, 259 p. https://doi.org/10.3133/ofr69202.

Peucker-Ehrenbrink, B., and Ravizza, G., 2000, The marine osmium isotope record: Terra Nova, v. 12, no. 5, p. 205-219, https://doi.org/10.1046/j.1365-3121.2000.00295.x.

Pratt, L., and Threlkeld, C., 1984, Stratigraphic significance of 13C/12C ratios in mid-Cretaceous rocks of the Western Interior, USA, *in* Stott, D. F., and Glass, D. J., eds., The Mesozoic of middle North America, Volume 9, Canadian Society of Petroleum Geologists Memoir, p. 305-312.

Pratt, L. M., 1984, Influence of paleoenvironmental factors on preservation of organic matter in Middle Cretaceous Greenhorn Formation, Pueblo, Colorado: AAPG Bulletin, v. 68, no. 9, p. 1146-1159, https://doi.org/10.1306/AD4616E7-16F7-11D7-8645000102C1865D.

Pratt, L. M., 1985, Isotopic studies of organic matter and carbonate in rocks of the Greenhorn Marine Cycle, *in* Pratt, L. M., Kauffman, E. G., and Zelt, F. B., eds., Fine-grained deposits and biofacies of the Cretaceous Western Interior Seaway: Evidence of cyclic sedimentary processes, Volume 4, SEPM Field Trip Guidebook, p. 38-48, https://doi.org/10.2110/sepmfg.04.038.

Pratt, L. M., Arthur, M. A., Dean, W. E., and Scholle, P. A., 1993, Paleoceanographic cycles and events during the Late Cretaceous in the Western Interior Seaway of North America, *in* Caldwell, W. G. E., and Kauffman, E. G., eds., Evolution of the Western Interior Basin, Volume Special Paper 39, Geological Association of Canada, p. 333-354.

Raven, M. R., Fike, D. A., Gomes, M. L., Webb, S. M., Bradley, A. S., and McClelland, H.-L. O., 2018, Organic carbon burial during OAE2 driven by changes in the locus of organic matter sulfurization: Nature Communications, v. 9, no. 1, p. 3409, https://doi.org/10.1038/s41467-018-05943-6.

Ravizza, G., and Peucker-Ehrenbrink, B., 2003, Chemostratigraphic Evidence of Deccan Volcanism from the Marine Osmium Isotope Record: Science, v. 302, no. 5649, p. 1392-1395, DOI: 10.1126/science.1089209.

Richardt, N., Wilmsen, M., and Niebuhr, B., 2013, Late Cenomanian–Early Turonian facies development and sea-level changes in the Bodenwöhrer Senke (Danubian Cretaceous Group, Bavaria, Germany): Facies, v. 59, no. 4, p. 803-827, https://doi.org/10.1007/s10347-012-0337-x.

Rivera, T. A., Schmitz, M. D., Crowley, J. L., and Storey, M., 2014, Rapid magma evolution constrained by zircon petrochronology and 40Ar/39Ar sanidine ages for the Huckleberry Ridge Tuff, Yellowstone, USA: Geology, v. 42, no. 8, p. 643-646, https://doi.org/10.1130/G35808.1.

Robaszynski, F., Gale, A. S., Juignet, P., Amedro, F., and Hardenbol, J., 1998, Sequence stratigraphy in the Upper Cretaceous Series of the Anglo-Paris Basin: expemplified by the Cenomanian Stage, *in* de Graciansky, P., Hardenbol, J., Jacquin, T., and Vail, P. R., eds., Mesozoic and Cenozoic Sequence Stratigraphy of European Basins, Volume 60, SEPM Special Publication, p. 363-386, https://doi.org/10.2110/pec.98.02.0363.

Roberts, L. N. R., and Kirschbaum, M. A., 1995, Paleogeography and the Late Cretaceous of the Western Interior of middle North America; coal distribution and sediment accumulation: U.S. Geological Survey Professional Paper 1561, 155 p., https://doi.org/10.3133/pp1561.

Rooney, A. D., Selby, D., Lloyd, J. M., Roberts, D. H., Lückge, A., Sageman, B. B., and Prouty, N. G., 2016, Tracking millennial-scale Holocene glacial advance and retreat using osmium isotopes: Insights from the Greenland ice sheet: Quaternary Science Reviews, v. 138, p. 49-61, https://doi.org/10.1016/j.quascirev.2016.02.021.

Sageman, B. B., 1985, High-resolution stratigraphy and paleobiology of the Hartland Shale Member: analysis of an oxygen-deficient epicontinental sea, *in* Pratt, L. M., Kauffman, E. G., and Zelt, F. B., eds., Fine-Grained Deposits and Biofacies of the Cretaceous Western Interior Seaway: Evidence of Cyclical Sedimentary Processes, Volume 4, SEPM Guidebook, p. 110-121, https://doi.org/10.2110/sepmfg.04.110.

Sageman, B. B., 1989, The benthic boundary biofacies model: Hartland Shale member, greenhorn formation (Cenomanian), western interior, North America: Palaeogeography, Palaeoclimatology, Palaeoecology, v. 74, no. 1, p. 87-110, https://doi.org/10.1016/0031-0182(89)90021-7.

Sageman, B. B., 1996, Lowstand tempestites: Depositional model for cretaceous skeletal limestones, Western Interior basin: Geology, v. 24, no. 10, p. 888-892, https://doi.org/10.1130/0091-7613(1996)024%3C0888:LTDMFC%3E2.3.CO;2.

Sageman, B. B., Lyons, T. W., and Joo, Y. J., 2014a, Geochemistry of fine-grained, organic carbon-rich facies, in Turekian, K.K., ed., Treatise on Geochemistry (Second Edition):

Oxford, UK, Elsevier, v. 9, p. 141–179, https://doi.org/10.1016/B978-0-08-095975-7.00706-3.

Sageman, B. B., Meyers, S. R., and Arthur, M. A., 2006, Orbital time scale and new C-isotope record for Cenomanian-Turonian boundary stratotype: Geology, v. 34, no. 2, p. 125-128, https://doi.org/10.1130/G22074.1.

Sageman, B. B., Rich, J., Arthur, M. A., Birchfield, G. E., and Dean, W. E., 1997, Evidence for Milankovitch periodicities in Cenomanian-Turonian lithologic and geochemical cycles, western interior USA: Journal of Sedimentary Research, v. 67, no. 2, p. 286-302, https://doi.org/10.1306/D4268554-2B26-11D7-8648000102C1865D.

Sageman, B. B., Singer, B. S., Meyers, S. R., Siewert, S. E., Walaszczyk, I., Condon, D. J., Jicha, B. R., Obradovich, J. D., and Sawyer, D. A., 2014b, Integrating Ar-40/Ar-39, U-Pb, and astronomical clocks in the Cretaceous Niobrara Formation, Western Interior Basin, USA: Geological Society of America Bulletin, v. 126, no. 7-8, p. 956-973, https://doi.org/10.1130/B30929.1.

Savrda, C. E., and Bottjer, D. J., 1994, Ichnofossils and Ichnofabrics in Rhythmically Bedded Pelagic/Hemi-Pelagic Carbonates: Recognition and Evaluation of Benthic Redox and Scour Cycles, *in* de Boer, P. L., and Smith, D. G., eds., Orbital Forcing and Cyclic Sequences: Oxford, p. 195-210, https://doi.org/10.1002/9781444304039.ch15.

Schlanger, S. O., Arthur, M. A., Jenkyns, H. C., and Scholle, P. A., 1987, The Cenomanian-Turonian Oceanic Anoxic Event, I. Stratigraphy and distribution of organic carbon-rich beds and the marine δ13C excursion: Geological Society, London, Special Publications, v. 26, no. 1, p. 371-399, https://doi.org/10.1144/GSL.SP.1987.026.01.24.

Schlanger, S. O., and Jenkyns, H. C., 1976, Cretaceous Oceanic Anoxic Events: Causes and Consequences: Geologie en Mijnbouw, v. 55, no. 3-4, p. 6.

Scholle, P. A., and Arthur, M. A., 1980, Carbon isotope fluctuations in Cretaceous pelagic limestones - potential stratigraphic and petroleum exploration tool: AAPG Bulletin, v. 64, no. 1, p. 67-87, https://doi.org/10.1306/2F91892D-16CE-11D7-8645000102C1865D.

Schröder-Adams, C. J., Herrle, J. O., Selby, D., Quesnel, A., and Froude, G., 2019, Influence of the High Arctic Igneous Province on the Cenomanian/Turonian boundary interval, Sverdrup Basin, High Canadian Arctic: Earth and Planetary Science Letters, v. 511, p. 76-88, https://doi.org/10.1016/j.epsl.2019.01.023.

Scott, R. W., Oboh-Ikuenobe, F. E., Benson, D. G., Holbrook, J. M., Alnahwi, A., 2018, Cenomanian-Turonian flooding cycles: U.S. Gulf Coast and Western Interior: Cretaceous Research, v. 89, p. 191-210, https://doi.org/10.1016/j.cretres.2018.03.027.

Selby, D., and Creaser, R. A., 2003, Re-Os geochronology of organic rich sediments: an evaluation of organic matter analysis methods: Chemical Geology, v. 200, no. 3-4, p. 225-240, https://doi.org/10.1016/S0009-2541(03)00199-2.

Singer, B. S., Jicha, B. R., Condon, D. J., Macho, A. S., Hoffman, K. A., Dierkhising, J., Brown, M. C., Feinberg, J. M., and Kidane, T., 2014, Precise ages of the Réunion event and Huckleberry Ridge excursion: Episodic clustering of geomagnetic instabilities and the dynamics of flow within the outer core: Earth and Planetary Science Letters, v. 405, p. 25-38, https://doi.org/10.1016/j.epsl.2014.08.011.

Sinton, C. W., and Duncan, R. A., 1997, Potential links between ocean plateau volcanism and global ocean anoxia at the Cenomanian-Turonian boundary: Economic Geology, v. 92, no. 7-8, p. 836-842, https://doi.org/10.2113/gsecongeo.92.7-8.836.

Smith, A. B., Gale, A. S., and Neale, E. A. M., 2001, Sea-Level Change and Rock-Record Bias in the Cretaceous: A Problem for Extinction and Biodiversity Studies: Paleobiology, v. 27, no. 2, p. 241-253, https://www.jstor.org/stable/2666072.

Smoliar, M. I., Walker, R. J., and Morgan, J. W., 1996, Re-Os ages of group IIA, IIIA, IVA, and IVB iron meteorites: Science, v. 271, no. 5252, p. 1099-1102, DOI: 10.1126/science.271.5252.1099.

Snow, L. J., Duncan, R. A., and Bralower, T. J., 2005, Trace element abundances in the Rock Canyon Anticline, Pueblo, Colorado, marine sedimentary section and their relationship to Caribbean plateau construction and oxygen anoxic event 2: Paleoceanography, v. 20, no. 3, https://doi.org/10.1029/2004PA001093.

Sullivan, D. L., Brandon, A. D., Eldrett, J., Bergman, Minisini, D., S. C., Wright, S. (in press) High Resolution Osmium Data Record Three Distinct Pulses of Magmatic Activity During Cretaceous Ocean Anoxic Event 2 (OAE 2): Geochimica et Cosmochimica Acta, https://doi.org/10.1016/j.gca.2020.04.002.

Tibert, N. E., Leckie, R. M., Eaton, J. G., Kirkland, J. I., Colin, J.-P., Leithold, E. L., and McCormic, M. E., 2003, Recognition of relative sea-level change in Upper Cretaceous coal-bearing strata: a paleoecological approach using agglutinated foraminifera and ostracodes to detect key stratigraphic surfaces, *in* C, O. H., and Leckie, R. M., eds., Micropaleontologic proxies for sea-level change and stratigraphic discontinuities, Volume 75, Society for Sedimentary Geology, p. 263-299, https://doi.org/10.2110/pec.03.75.0263.

Tsikos, H., Jenkyns, H. C., Walsworth-Bell, B., Petrizzo, M. R., Forster, A., Kolonic, S., Erba, E., Silva, I. P., Baas, M., Wagner, T., and Damste, J. S. S., 2004, Carbon-isotope stratigraphy recorded by the Cenomanian-Turonian Oceanic Anoxic Event: correlation and implications based on three key localities: Journal of the Geological Society, v. 161, p. 711-719, https://doi.org/10.1144/0016-764903-077.

Turgeon, S. C., and Creaser, R. A., 2008, Cretaceous oceanic anoxic event 2 triggered by a massive magmatic episode: Nature, v. 454, no. 7202, p. 323-U329, https://doi.org/10.1038/nature07076.

Uličný, D., 1999, Sequence stratigraphy of the Dakota Formation (Cenomanian), southern Utah: interplay of eustasy and tectonics in a foreland basin: Sedimentology, v. 46, no. 5, p. 807-836, https://doi.org/10.1046/j.1365-3091.1999.00252.x.

Uličný, D., Hladíková, J., Attrep, M. J., Čech, S., Hradecká, L., and Svobodová, M., 1997, Sea-level changes and geochemical anomalies across the Cenomanian-Turonian boundary: Pecinov quarry, Bohemia: Palaeogeography Palaeoclimatology Palaeoecology, v. 132, no. 1-4, p. 265-285, https://doi.org/10.1016/s0031-0182%2897%2900055-2.

Voigt, S., Gale, A. S., and Voigt, T., 2006, Sea-level change, carbon cycling and palaeoclimate during the Late Cenomanian of northwest Europe; an integrated palaeoenvironmental analysis: Cretaceous Research, v. 27, no. 6, p. 836-858, https://doi.org/10.1016/j.cretres.2006.04.005.

Wendler, J. E., Meyers, S. R., Wendler, I., and Kuss, J., 2014, A million-year-scale astronomical control on Late Cretaceous sea-level: Newsletters on Stratigraphy, v. 47, no. 1, p. 1-19, https://doi.org/10.1127/0078-0421/2014/0038.

Wignall, P. B., 2001, Large igneous provinces and mass extinctions: Earth-Science Reviews, v. 53, no. 1, p. 1-33, https://doi.org/10.1016/S0012-8252(00)00037-4.

Wotzlaw, J.-F., Schaltegger, U., Frick, D. A., Dungan, M. A., Gerdes, A., and Günther, D., 2013, Tracking the evolution of large-volume silicic magma reservoirs from assembly to supereruption: Geology, v. 41, no. 8, p. 867-870, https://doi.org/10.1130/G34366.1.

Wu, H., Zhang, S., Jiang, G., Hinnov, L., Yang, T., Li, H., Wan, X., and Wang, C., 2013, Astrochronology of the Early Turonian-Early Campanian terrestrial succession in the Songliao Basin, northeastern China and its implication for long-period behavior of the Solar System: Palaeogeography Palaeoclimatology Palaeoecology, v. 385, p. 55-70, https://doi.org/10.1016/j.palaeo.2012.09.004.

Young, R. G., 1965, Type section of Naturita Formation: AAPG Bulletin, v. 49, no. 9, p. 1512-1516, https://doi.org/10.1306/A663372E-16C0-11D7-8645000102C1865D.

Figure Captions

Figure 1. Early Turonian map of North American Western Interior Basin marking primary localities of cores investigated or discussed in this study (adapted from Roberts and Kirschbaum, 1995; Ma et al., 2014). AZ-Arizona, USA; CO-Colorado, USA; GSSP-global boundary stratotype section and point; NC-Nipple Creek outcrop; SH#1 – Smoky Hollow #1 Core.

Figure 2. Lithostratigraphy and ammonite biostratigraphy of the Cenomanian-Turonian boundary interval in the Western Interior Basin from central Colorado to southern Utah (modified from Tibert et al., 2003). Regional bentonites of Elder (1988) and Leithold (1994). Shoreline trajectory of genetic sequences scaled versus age (modified from Laurin et al., 2019). Ls.-limestone; OAE2-Oceanic Anoxic Event 2; Ss-sandstone; GSSP-global boundary stratotype section and point; SH#1 – Smoky Hollow #1 Core.

Figure 3. Chemostratigraphy of the Angus Core. From left to right: wt.% carbonate content and wt.% total organic carbon (TOC) (open circles = new data in Data Repository, black/blue circles from Joo and Sageman, 2014), bulk organic carbon isotopic ratios $\delta^{13}C_{org}$ (Joo and Sageman, 2014), initial osmium isotope ratios Os_i, rhenium concentrations (green circles), 192-osmium concentrations (orange squares) (Table 1). Mbr.-member; OAE2-Oceanic Anoxic Event 2.

Figure 4. Chemostratigraphy of the Smoky Hollow (SH#1) Core in southern Utah. From left to right: wt.% carbonate content, wt.% total organic carbon (TOC), and bulk organic carbon isotope ratios ($\delta^{13}C_{org}$) from Jones et al. (2019); $^{40}Ar/^{39}Ar$ bentonite ages, initial osmium isotope ratios (Os_i), rhenium concentrations (green circles), and 192-osmium concentrations (orange squares) from this study. $^{40}Ar/^{39}Ar$ bentonite dates correlated from the nearby Nipple Creek outcrop section. Stratigraphic column, correlated ammonite biostratigraphy, bentonite stratigraphy, and

Cenomanian-Turonian boundary placement updated (see Fig. DR3 in Data Repository) from Jones et al. (2019). See text for discussion. Lithology legend in Fig. 5. Fm.-formation; fs-flooding surface; OAE2-Oceanic Anoxic Event 2; VPDB-Vienna Pee Dee belemnite; P.f.-*Pseudaspidoceras flexuosum*.

Figure 5. Initial osmium isotope records of the Western Interior Basin. Stratigraphic columns for the SH#1 Core (updated from Jones et al., 2019), Angus Core (this study), Portland Core near GSSP (Meyers et al., 2012b), and Iona-1 Core from the Maverick Basin, Texas (redrafted from Eldrett et al., 2015) (L-R). Bentonite labels A-D in red for central WIB sites; these bentonites may be present in the Iona-1 Core of Texas, however, they were originally reported to pinch out in New Mexico before reaching Texas (Elder, 1988), complicating exact bentonite correlations to the Iona-1 Core. Bandpass filters for the SH#1 (Jones et al., 2019), Angus (Ma et al., 2014), Portland (Meyers et al., 2012b), and Iona-1 cores (Eldrett et al., 2015). Quantified durations of Portland Core/GSSP hiatuses from Meyers and Sageman (2004) and this study (see Results). Carbon isotope ($\delta^{13}C_{org}$) chemostratigraphy in black for the SH#1 (Jones et al., 2019), Angus (Joo and Sageman, 2014), Portland (Sageman et al., 2006; Du Vivier et al., 2014), and Iona-1 cores (Eldrett et al., 2015) define the OAE2 excursion (dark grey shading=short, end of plateau definition; light grey and dark grey shading=long definition). Initial osmium isotope ratios (Os_i) (open circles/red line) preserve unradiogenic (hydrothermal/LIP) excursion underlying OAE2 for SH#1 and Angus cores (this study), Portland Core (Du Vivier et al., 2014), and Iona-1 Core (Sullivan et al., in press). Fm.-formation; OAE2-Oceanic Anoxic Event 2.

Figure 6. Timeseries of $\delta^{13}C_{org}$ and Re-Os geochemical records from the SH#1 (light red), Angus (blue), and Portland (black) cores through OAE2. Break in Portland Core timeseries during lag (grey) signifies hiatus. From left to right, figure plots bulk carbon isotope ratios ($\delta^{13}C_{org}$), initial

osmium isotope composition (Os_i), osmium-192 concentration, and rhenium concentration. Timeseries for Angus Core from astrochronology (Ma et al., 2014), Portland Core from astrochronology (Meyers et al., 2001) and linear interpolation of ammonite biozones below hiatus (this study), and SH#1 Core from astrochronology (Jones et al., 2019) and linear interpolation of sedimentation rates below OAE2 CIE. See text for methods and discussion. OAE2-Oceanic Anoxic Event 2.

Figure 7. Left - Plot of all recent $^{40}Ar/^{39}Ar$ (circles) and CA-ID-TIMS U-Pb (squares) ages for the B, C, and D bentonites in the Western Interior Basin. Right - recent age estimates for the Cenomanian-Turonian boundary (CTB), including the GTS2012 age from Meyers et al. (2012b). Filled circles represent data from this study. All data are shown with 2σ full external uncertainties. Note that U-Pb dates of Meyers et al. (2012b) from Lohali Point, Arizona for bentonites C and D are not plotted due to the presence of inherited zircons, similar to trends exhibited in several plotted U-Pb ages for Bentonite B. The Eldrett et al. (2015) youngest zircon date for bentonite “B4” is from a horizon that is 0.5-1.0 short eccentricity cycle below where they place Bentonite B and thus is not considered further when discussing age calculations (see Eldrett et al., 2015 supplement for details). The age from “Bighorn River (n=6)” corresponds to the age derived from all six zircons analyzed from the bentonite sample, whereas “Bighorn River (n=3)” corresponds to the youngest three zircon ages from the horizon (Barker et al., 2011). Several samples possessing inherited zircons or considered outliers (diamonds) are not included in the calculation of the weighted mean age of the Cenomanian-Turonian boundary for this study (grey shading and dashed line). See text, Table 2, and Table DR1 in Data Repository for determination of the CTB age.

Figure 8. Refined conceptual timeline of OAE2. From left to right – sea level history during OAE2 (Jones et al., 2019) and isotopic records of osmium (this study), calcium (Du Vivier et al., 2015a), thallium (Ostrander et al., 2017), and carbon (Joo and Sageman, 2014) as proxies for LIP volcanic activity, carbonate chemistry, marine deoxygenation, and carbon cycle response of organic carbon burial, respectively. Dashed line in δ^{44}Ca profile reflects missing time in Portland Core. Data from other sites and within and outside WIB confirm coincident timing of δ^{44}Ca and Os_i excursions. See text for discussion**.**

TABLE CAPTIONS

Table 1. RHENIUM-OSMIUM GEOCHEMISTRY OF THE ANGUS AND SH#1 CORES THROUGH OCEANIC ANOXIC EVENT 2.

TABLE 2. SUMMARY OF ^{40}AR/^{39}AR AGE DATA FOR BENTONITES B, C, AND D AT NIPPLE CREEK (NC) OUTCROP, UTAH, USA; LOHALI POINT, ARIZONA, USA; AND PUEBLO, COLORADO, USA.

[1]GSA Data Repository item 20XXxxx, (1) Complete Ar geochronology data, bentonite correlations and collection in Kaiparowits Plateau, Cenomanian-Turonian boundary age calculations, core photos and description of hiatuses, and Angus Core depth scale alignment correction; (2) Time scale tables for cores, is available online at www.geosociety.org/pubs/ft20xx.htm, or on request from editing@geosociety.org.

Figure 1

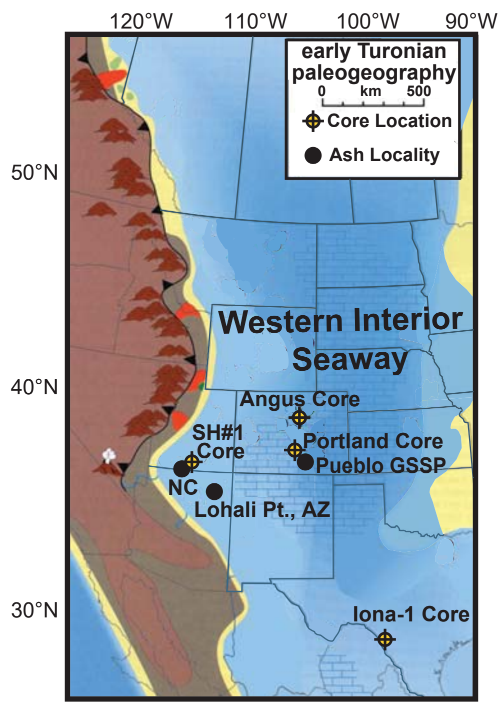

120°W
110°W
100°W
90°W
50°N
40°N
30°N
early Turonian paleogeography
0 km 500
Core Location
Ash Locality
Western Interior Seaway
Angus Core
SH#1 Core
Portland Core
Pueblo GSSP
NC
Lohali Pt., AZ
Iona-1 Core

Figure 2

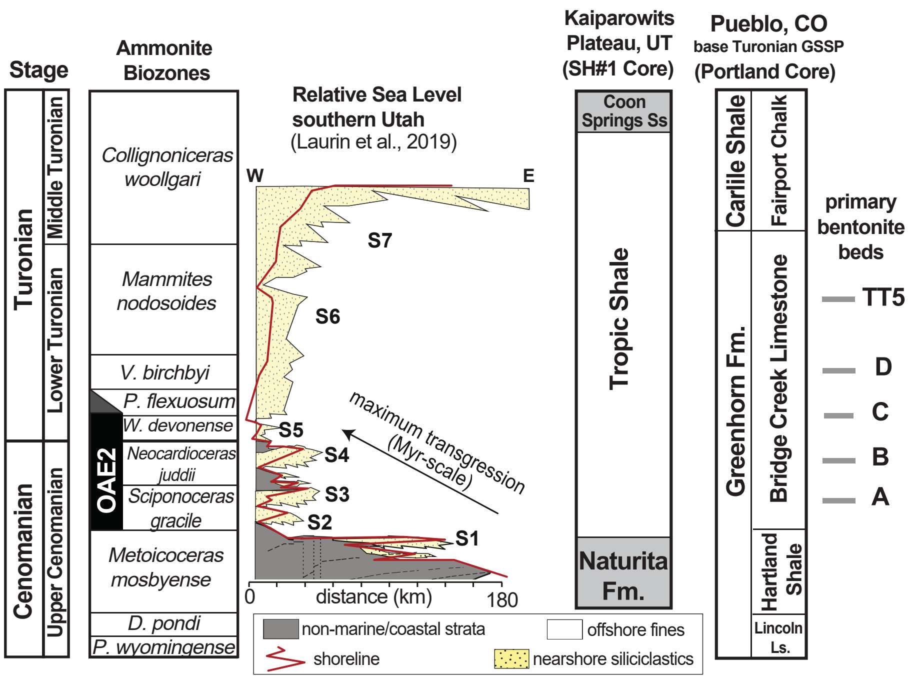

Stage
Turonian
Middle Turonian
Lower Turonian
Cenomanian
Upper Cenomanian
Ammonite Biozones
Collignoniceras woollgari
Mammites nodosoides
V. birchbyi
P. flexuosum
W. devonense
OAE2
Neocardioceras juddii
Sciponoceras gracile
Metoicoceras mosbyense
D. pondi
P. wyomingense
Relative Sea Level southern Utah
(Laurin et al., 2019)
W
E
S7
S6
S5
S4
S3
S2
S1
maximum transgression (Myr-scale)
0
distance (km)
180
non-marine/coastal strata
offshore fines
shoreline
nearshore siliciclastics
Kaiparowits Plateau, UT (SH#1 Core)
Coon Springs Ss
Tropic Shale
Naturita Fm.
Pueblo, CO
base Turonian GSSP
(Portland Core)
Carlile Shale
Fairport Chalk
Greenhorn Fm.
Bridge Creek Limestone
Hartland Shale
Lincoln Ls.
primary bentonite beds
TT5
D
C
B
A

Figure 3

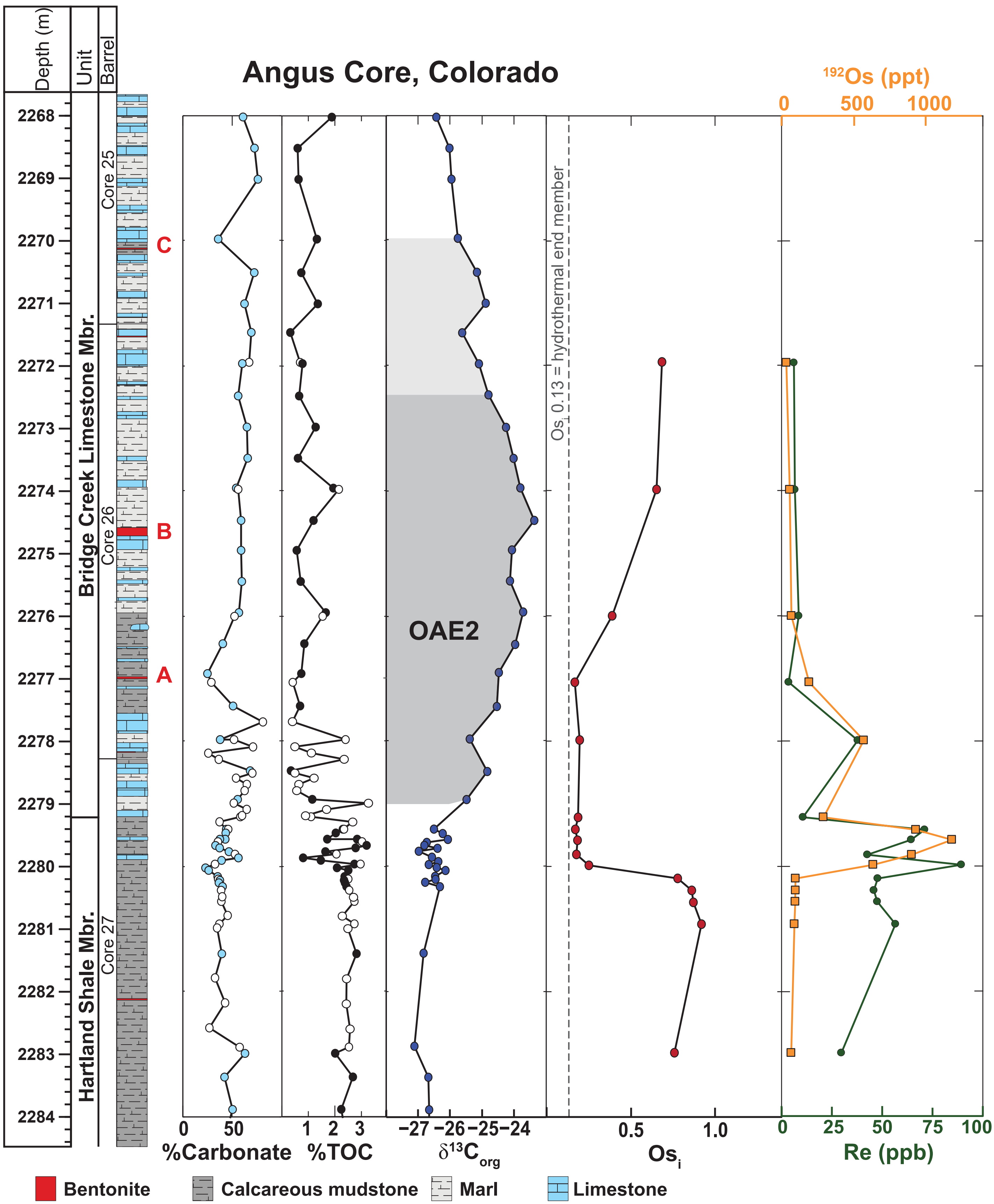

Angus Core, Colorado
Depth (m)
Unit
Barrel
Bridge Creek Limestone Mbr.
Hartland Shale Mbr.
Core 25
Core 26
Core 27
C
B
A
OAE2
Os$_i$ 0.13 = hydrothermal end member
%Carbonate
%TOC
$\delta^{13}C_{org}$
Os$_i$
^{192}Os (ppt)
Re (ppb)
Bentonite
Calcareous mudstone
Marl
Limestone

Figure 4

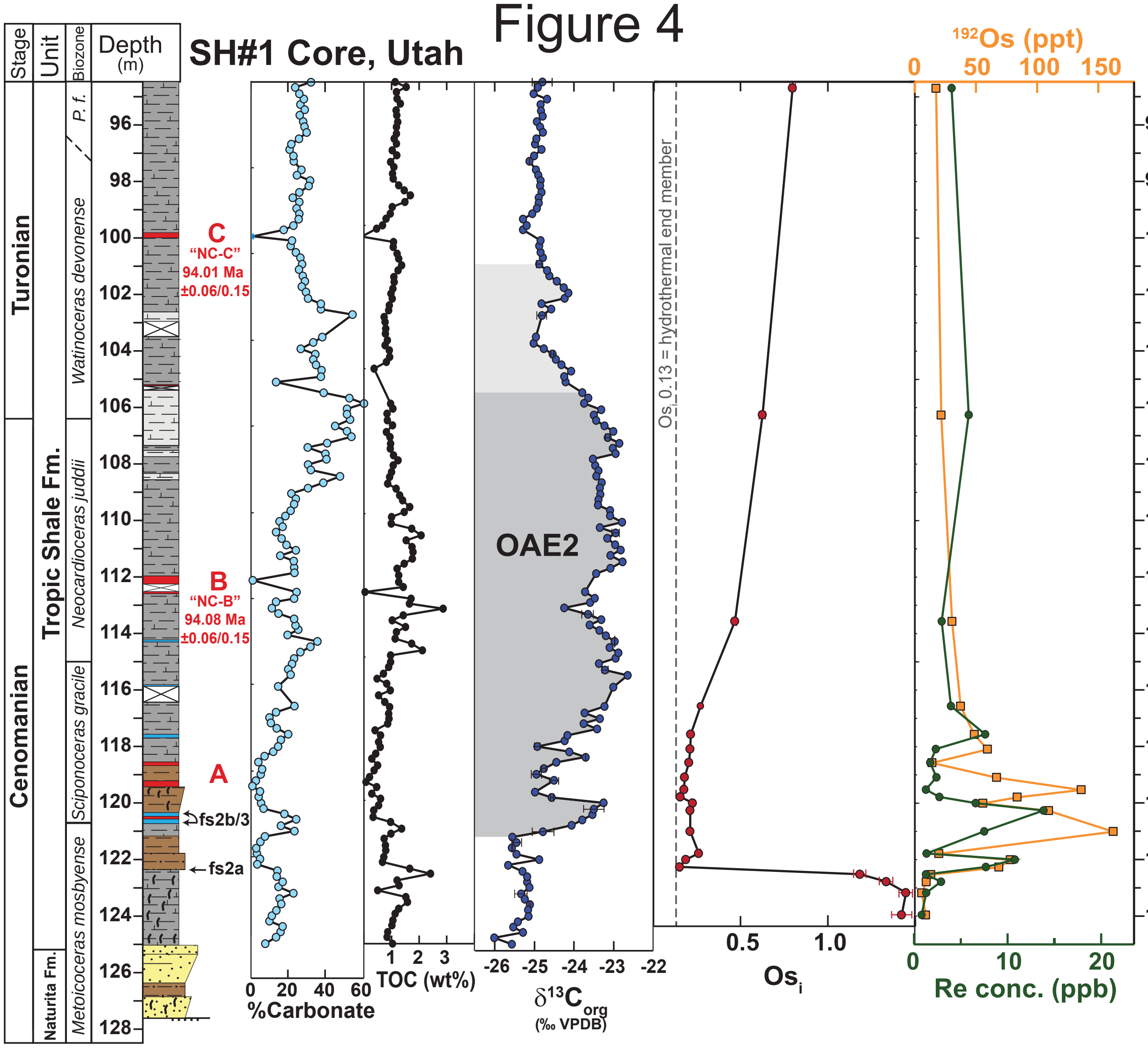

SH#1 Core, Utah
Stage
Unit
Biozone
Depth (m)
Turonian
Cenomanian
Tropic Shale Fm.
Naturita Fm.
P. f.
Watinoceras devonense
Neocardioceras juddii
Sciponoceras gracile
Metoicoceras mosbyense
C
"NC-C"
94.01 Ma
±0.06/0.15
B
"NC-B"
94.08 Ma
±0.06/0.15
A
fs2b/3
fs2a
%Carbonate
TOC (wt%)
OAE2
δ13Corg (‰ VPDB)
Osi 0.13 = hydrothermal end member
Osi
192Os (ppt)
Re conc. (ppb)

Figure 5

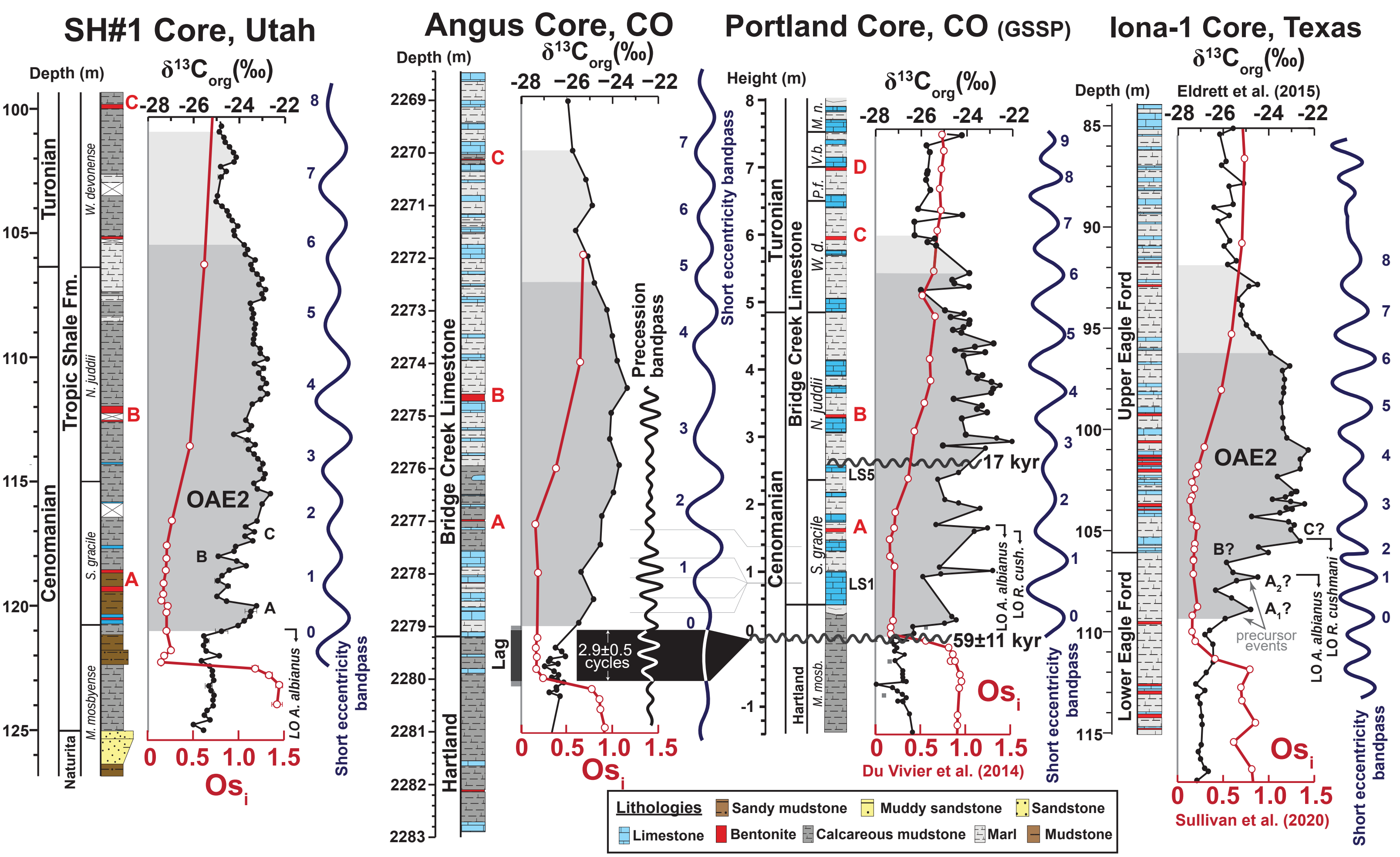

SH#1 Core, Utah
Angus Core, CO
Portland Core, CO (GSSP)
Iona-1 Core, Texas
δ13Corg(‰)
Depth (m)
Height (m)
Turonian
Cenomanian
Tropic Shale Fm.
Naturita
Bridge Creek Limestone
Hartland
Upper Eagle Ford
Lower Eagle Ford
OAE2
Osi
Short eccentricity bandpass
Precession bandpass
LO A. albianus
LO R. cushmani
LO R. cush.
2.9±0.5 cycles
Lag
17 kyr
59±11 kyr
precursor events
Du Vivier et al. (2014)
Sullivan et al. (2020)
Eldrett et al. (2015)
Lithologies
Sandy mudstone
Muddy sandstone
Sandstone
Limestone
Bentonite
Calcareous mudstone
Marl
Mudstone

Figure 6

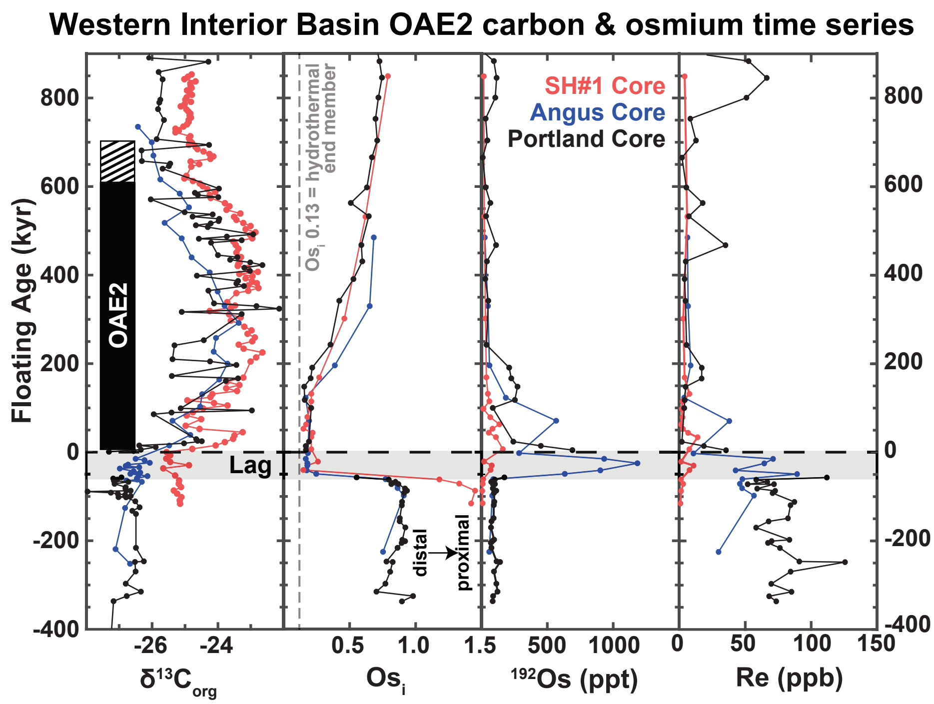

Western Interior Basin OAE2 carbon & osmium time series
Floating Age (kyr)
OAE2
Lag
Os$_i$ 0.13 = hydrothermal end member
distal
proximal
SH#1 Core
Angus Core
Portland Core
δ^{13}C$_{org}$
Os$_i$
^{192}Os (ppt)
Re (ppb)

Figure 7

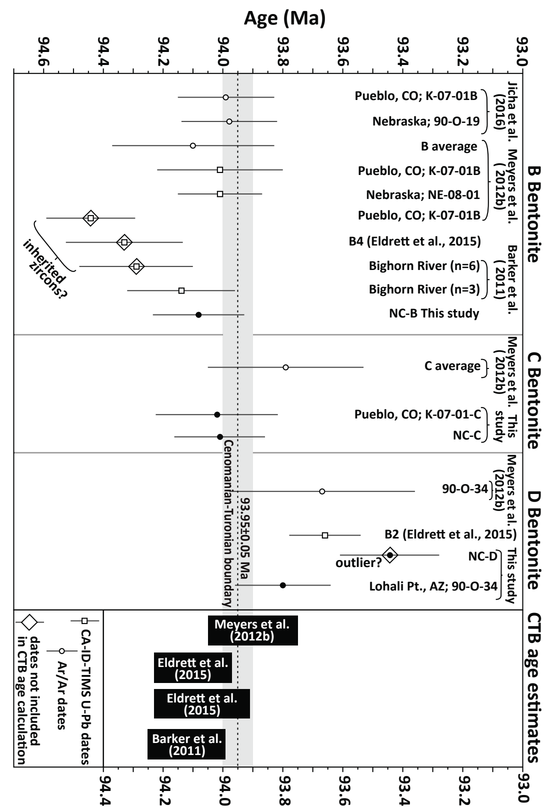

Age (Ma)
B Bentonite
C Bentonite
D Bentonite
CTB age estimates
Jicha et al. (2016)
Pueblo, CO; K-07-01B
Nebraska; 90-O-19
Meyers et al. (2012b)
B average
Pueblo, CO; K-07-01B
Nebraska; NE-08-01
Pueblo, CO; K-07-01B
B4 (Eldrett et al., 2015)
Barker et al. (2011)
Bighorn River (n=6)
Bighorn River (n=3)
NC-B This study
inherited zircons?
C average
This study
Pueblo, CO; K-07-01-C
NC-C
90-O-34
B2 (Eldrett et al., 2015)
NC-D
outlier?
Lohali Pt., AZ; 90-O-34
93.95±0.05 Ma
Cenomanian-Turonian boundary
Meyers et al. (2012b)
Eldrett et al. (2015)
Eldrett et al. (2015)
Barker et al. (2011)
CA-ID-TIMS U-Pb dates
Ar/Ar dates
dates not included in CTB age calculation

Figure 8

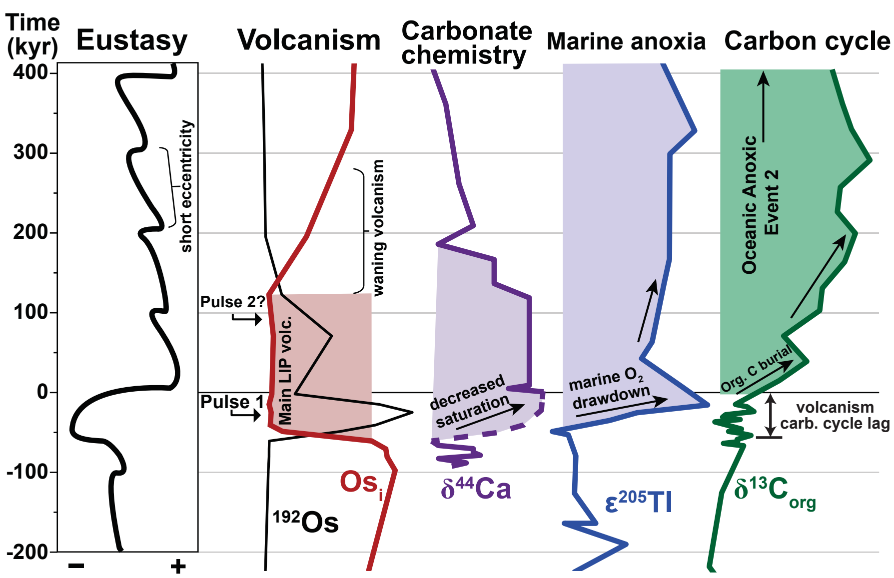

Time (kyr)
Eustasy
Volcanism
Carbonate chemistry
Marine anoxia
Carbon cycle
400
300
200
100
0
-100
-200
−
+
short eccentricity
waning volcanism
Pulse 2?
Pulse 1
Main LIP volc.
Os$_i$
^{192}Os
decreased saturation
δ^{44}Ca
marine O_2 drawdown
ε^{205}Tl
Oceanic Anoxic Event 2
Org. C burial
volcanism carb. cycle lag
$\delta^{13}C_{org}$

TABLE 1. RHENIUM-OSMIUM GEOCHEMISTRY OF THE ANGUS AND SH#1 CORES THROUGH OCEANIC ANOXIC

Angus Core Samples	Depth (m)	Re (ppb)	±	Os (ppt)	±	^{192}Os (ppt)	±	^{187}Re/^{188}Os	±	$^{187/188}$Os	±
RO750-1_AA7454'-2.5cm	2271.95	6.15	0.02	71.8	0.4	25.3	0.2	483.7	3.3	1.444	0.012
RO745-1_AA7460'+17cm	2273.98	6.62	0.02	133.3	0.6	49.0	0.2	269.0	1.5	1.076	0.007
RO750-2_AA7467'+5.5cm	2276.00	8.54	0.02	161.0	0.7	60.9	0.3	279.0	1.7	0.827	0.006
RO750-3_AA7471'-10.5cm	2277.06	3.55	0.01	453.4	1.4	184.8	1.0	38.3	0.2	0.227	0.002
RO745-2_AA7474'-9cm	2277.99	37.88	0.09	1422.6	4.2	567.0	2.2	132.9	0.6	0.402	0.002
RO745-3_AA7477'+3cm	2279.22	10.66	0.03	708.1	2.3	285.9	1.5	74.2	0.4	0.300	0.002
RO750-4_AA7478'-7cm	2279.42	71.09	0.18	2338.2	6.5	931.4	3.4	151.8	0.7	0.407	0.002
RO750-5_AA7478'+9cm	2279.58	64.41	0.16	2951.0	7.8	1183.9	4.3	108.2	0.5	0.350	0.002
RO745-4_AA7479'+2cm	2279.82	42.64	0.11	2241.1	6.2	902.2	3.6	94.0	0.4	0.323	0.002
RO750-6_AA7479'+18cm	2279.98	89.31	0.22	1644.6	5.3	632.6	2.2	280.9	1.2	0.689	0.003
RO745-5_AA7480'+9.5cm	2280.20	47.78	0.12	282.9	1.5	89.7	0.4	1059.1	5.2	2.439	0.014
RO750-7_AA7481'-1.5cm	2280.39	45.86	0.12	278.4	1.5	87.9	0.4	1038.2	5.1	2.489	0.014
RO745-6_AA7481'+16cm	2280.57	47.57	0.12	279.8	1.5	87.7	0.4	1079.5	5.3	2.562	0.015
RO750-8_AA7483'-8.5cm	2280.93	56.60	0.14	274.9	1.6	82.0	0.3	1373.0	6.6	3.071	0.017
RO745-7_AA7489'+14.5cm	2282.99	29.72	0.08	185.2	1.0	59.5	0.3	994.4	5.1	2.318	0.014

SH#1 Core Samples	Depth (m)	Re (ppb)	±	Os (ppt)	±	^{192}Os (ppt)	±	^{187}Re/^{188}Os	±	$^{187/188}$Os	±
RO751-1_SH#1-94.66m	94.66	4.03	0.01	50.7	0.3	17.7	0.1	451.3	2.9	1.504	0.012
RO751-2_SH#1-106.27m	106.27	5.86	0.02	61.4	0.3	21.6	0.1	540.2	3.3	1.471	0.011
RO751-3_SH#1-113.58m	113.58	2.96	0.01	79.9	0.5	30.5	0.3	193.1	1.8	0.768	0.010
RO751-4_SH#1-116.58m	116.58	3.95	0.01	96.2	0.4	37.4	0.2	209.9	1.3	0.600	0.005
RO751-5_SH#1-117.58m	117.58	7.64	0.02	126.5	0.5	48.6	0.3	312.8	1.8	0.701	0.005
RO751-6_SH#1-118.08m	118.08	2.35	0.01	148.7	0.7	59.8	0.5	78.0	0.7	0.330	0.004
RO751-7_SH#1-118.58m	118.58	1.76	0.01	36.2	0.2	14.1	0.1	248.9	2.5	0.593	0.008
RO751-8_SH#1-119.08m	119.08	2.41	0.01	165.5	0.8	66.9	0.6	71.8	0.7	0.291	0.004
RO741-6_SH1: 119.53m	119.53	1.27	0.01	333.2	3.2	136.2	2.8	18.5	0.4	0.204	0.006
RO741-7_SH1: 119.79m	119.79	2.72	0.01	206.6	1.1	83.9	0.9	64.6	0.7	0.255	0.004
RO751-9_SH#1-120.03m	120.03	6.60	0.02	143.1	0.6	55.7	0.3	235.8	1.4	0.591	0.004
RO703-1_SH1-35:7	120.29	13.86	0.04	282.4	1.2	109.8	0.6	251.1	1.5	0.603	0.005
RO703-2_SH1-35:10	121.03	7.52	0.02	404.8	1.4	162.3	0.9	92.2	0.6	0.355	0.003
RO703-3_SH1-35:12	121.78	1.34	0.01	50.0	0.4	19.8	0.3	134.7	2.0	0.470	0.009
RO741-8_SH1: 122.02m	122.02	10.79	0.03	201.6	0.8	78.2	0.4	274.2	1.7	0.615	0.005
RO741-9_SH1: 122.29m	122.29	7.68	0.02	175.4	0.7	69.1	0.4	221.2	1.4	0.497	0.004
RO741-10_SH1: 122.53m	122.53	1.30	0.01	38.0	0.4	13.3	0.2	193.9	2.9	1.488	0.029
RO703-4_SH1-36:1	122.78	2.91	0.01	29.9	0.3	9.7	0.1	599.3	6.1	2.275	0.030
RO751-10_SH#1-123.21m	123.21	1.32	0.01	18.2	0.2	6.0	0.1	438.9	5.4	2.137	0.030
RO703-5_SH1-36:3	123.98	0.81	0.01	26.0	0.3	8.9	0.2	181.7	4.1	1.710	0.050

Notes:

[a]Initial osmium isotope ratios (Osi) are calculated using an age of 94.4 Ma

[b]T=0 for the floating time scale is placed at the base of the carbon isotope excursion of Oceanic Anoxic Event 2

C EVENT 2 INTERVAL

rho	Os_i[a]	±	Floating[b] time (kyr)
0.673	0.683	0.017	475
0.605	0.652	0.009	320
0.633	0.388	0.009	186
0.612	0.167	0.002	113
0.590	0.193	0.003	61
0.627	0.184	0.003	-12
0.581	0.168	0.003	-25
0.578	0.180	0.003	-35
0.594	0.175	0.002	-51
0.574	0.247	0.005	-59
0.627	0.772	0.022	-71
0.624	0.855	0.022	-81
0.628	0.863	0.023	-91
0.625	0.910	0.027	-108
0.656	0.755	0.022	-235

rho	Os_i[a]	±	Floating[b] time (kyr)
0.653	0.794	0.016	849
0.654	0.620	0.017	532
0.666	0.464	0.012	302
0.623	0.270	0.007	169
0.639	0.209	0.008	132
0.654	0.207	0.005	115
0.651	0.201	0.012	98
0.654	0.178	0.005	79
0.683	0.175	0.006	63
0.663	0.154	0.005	53
0.633	0.220	0.007	44
0.626	0.207	0.007	34
0.612	0.210	0.004	7
0.665	0.258	0.012	-26
0.634	0.183	0.007	-36
0.615	0.149	0.006	-48
0.670	1.183	0.034	-59
0.703	1.331	0.039	-70
0.707	1.446	0.039	-90
0.670	1.424	0.057	-124

TABLE 2. SUMMARY OF $^{40}AR/^{39}AR$ DATA AND CENOMANIAN-TURONIAN BOUNDARY AGE

Sample	Locality	Latitude	Longitude	N	MSWD	Weighted mean Age (Ma)	±2σ[a]	±2σ[b]
Single sanidine incremental heating								
NC-D	Nipple Creek outcrop, UT	37.123	-111.672	10/11	1.40	93.443	± 0.090	± 0.166
NC-C	Nipple Creek outcrop, UT	37.122	-111.673	8/12	0.35	94.011	± 0.060	± 0.152
NC-B	Nipple Creek outcrop, UT	37.121	-111.672	10/11	1.20	94.082	± 0.057	± 0.152
Single sanidine fusions								
K-07-01-C	Pueblo, CO, USA	38.28	-104.74	20/20	1.12	94.022	± 0.147	± 0.204
90-O-34	Lohali Point, AZ, USA	36.185	-109.884	24/27	1.15	93.799	± 0.065	± 0.154

Notes:

Ages calculated relative to 28.201 Ma Fish Canyon sanidine (Kuiper et al. 2008) using decay constants of Min et al. (2000)

[a] Age uncertainty includes analytical uncertainty + J uncertainty.

[b] Total age uncertainty includes decay constrant, standard age, J, and analytical uncertainties.

[c] CTB age calculated by anchoring Portland Core astronomical timescale to ash date

[d] CTB age uncertainty includes radioisotopic, stage boundary placement, and astrochronological time scale uncertainties combined in quadrature.

For single crystal incremental heating experiments, N = number of plateau ages/number of experiments

For single crystal fusion data, N = number of dates included in weighted mean/number of fusions

Ages for the Cenomanian-Turonian Boundary are calculated by anchoring the floating astronomical time scale of the SH#1 Core to the new $^{40}Ar/^{39}Ar$ ages (see text for discussion).

CTB age (Ma)[c]	±2σ[d]
n/a	n/a
94.129	± 0.156
93.914	± 0.156
94.140	± 0.207
94.065	± 0.158